Sensitivity of Storm Surge Predictions to Atmospheric Forcing during Hurricane Isaac

J. C. Dietrich, Aff.M.ASCE[1]; A. Muhammad[2]; M. Curcic[3]; A. Fathi[4]; C. N. Dawson[5]; S. S. Chen[6]; and R. A. Luettich Jr.[7]

Abstract: Storm surge and overland flooding can be predicted with computational models at high levels of resolution. To improve efficiency in forecasting applications, surge models often use atmospheric forcing from parametric vortex models, which represent the surface pressures and wind fields with a few storm parameters. The future of storm surge prediction could involve real-time coupling of surge and full-physics atmospheric models; thus, their accuracies must be understood in a real hurricane scenario. The authors compare predictions from a parametric vortex model (using forecast tracks from the National Hurricane Center) and a full-physics coupled atmosphere-wave-ocean model during Hurricane Isaac (2012). The predictions are then applied within a tightly coupled, wave and surge modeling system describing the northern Gulf of Mexico and the floodplains of southwest Louisiana. It is shown that, in a hindcast scenario, a parametric vortex model can outperform a data-assimilated wind product, and given reasonable forecast advisories, a parametric vortex model gives reasonable surge forecasts. However, forecasts using a full-physics coupled model outperformed the forecast advisories and improved surge forecasts. Both approaches are valuable for forecasting the coastal impacts associated with tropical cyclones. **DOI: 10.1061/(ASCE)WW.1943-5460.0000419.**

Author keywords: ADCIRC; HWind; Generalized asymmetric Holland model (GAHM); unified wave interface coupled model (UWIN-CM).

Introduction

The northern Gulf of Mexico is an active region for hurricanes. In the last 12 years, the northern Gulf has been impacted by several storms including Katrina (2005), Gustav (2008), and Isaac (2012), each of which caused surge to develop on the Louisiana-Mississippi continental shelf and flooding to occur along the coasts of Louisiana, Mississippi, and Alabama (Knabb et al. 2005; Beven and Kimberlain 2009; Berg 2013). Katrina was the most devastating in loss of life and property. Gustav and Isaac caused less damage due to their relative sizes and tracks through Louisiana, as well as recent improvements in the protection systems surrounding the New Orleans metropolitan region.

Computational models can predict the impacts of these storms. Recent advancements in modeling of storm-induced waves and flooding have included the development, application, and validation of high-resolution, high-fidelity models along the entire Gulf coastline. These models are useful for long-term planning, such as the evaluation and design of surge barriers in Louisiana by the U.S. Army Corps of Engineers (Ebersole et al. 2007) or the development of floodplain risk maps for FEMA (Westerink 2008). They are also useful for scientific studies of the coastal environment, such as the effects of marshes and wetland restoration on the attenuation of storm surge (Wamsley et al. 2010). During a storm event, these models can provide guidance about where, when, and for how long the hazardous conditions will occur, assisting emergency managers in making decisions about resource deployment and evacuation (Cheung et al. 2003). However, model uncertainties are larger in a forecasting application. In addition to internal uncertainties due to input parameterizations (e.g., bathymetry and topography, bottom roughness, momentum transfer from the winds), the model is also subject to uncertainties in the storm's forecast of size, intensity, and landfall location.

Surge modeling systems have attempted to account for these uncertainties by moving toward probabilistic forecasting, in which guidance is developed from a suite of simulations, each with a slight variation on possible storm parameters (Glahn et al. 2009; Forbes and Rhome 2012). Maps can be provided with predicted flooding levels and their associated likelihoods (Zachry et al. 2015). This probabilistic guidance relies on the computational efficiency of individual simulations, but can be less accurate per simulation due to the coarse representation of the coastal environment and lack of wave forcing (Kerr et al. 2015). Recent advances in storm surge

[1]Assistant Professor, Dept. of Civil, Construction, and Environmental Engineering, North Carolina State University, 2501 Stinson Dr., Raleigh, NC 27607 (corresponding author). E-mail: jcdietrich@ncsu.edu

[2]Project Manager, United Airlines, 165 W Superior St., Apt. 2903, Chicago, IL 60654. E-mail: adnan.muhammad@utexas.edu

[3]Postdoctoral Researcher, Rosenstiel School of Marine and Atmospheric Science, Univ. of Miami, 4600 Rickenbacker Causeway, Miami, FL 33149. E-mail: milan@orca.rsmas.miami.edu

[4]Postdoctoral Researcher, Institute for Computational Engineering and Sciences, Univ. of Texas at Austin, 201 East 24th St., Stop C0200, Austin, TX 78712. E-mail: arash.fathi@utexas.edu

[5]Professor, Institute for Computational Engineering and Sciences, Univ. of Texas at Austin, 201 East 24th St., Stop C0200, Austin, TX 78712. E-mail: clint@ices.utexas.edu

[6]Professor, Rosenstiel School of Marine and Atmospheric Science, Univ. of Miami, 4600 Rickenbacker Causeway, Miami, FL 33149. E-mail: schen@rsmas.miami.edu

[7]Professor, Institute of Marine Sciences, Univ. of North Carolina at Chapel Hill, 3431 Arendell St., Morehead City, NC 28557. E-mail: rick_luettich@unc.edu

Note. This manuscript was submitted on December 21, 2016; approved on June 6, 2017; published online on October 12, 2017. Discussion period open until March 12, 2018; separate discussions must be submitted for individual papers. This paper is part of the ***Journal of Waterway, Port, Coastal, and Ocean Engineering***, © ASCE, ISSN 0733-950X.

prediction (Resio and Westerink 2008; Westerink et al. 2008) have produced high-resolution models (Luettich and Westerink 2004; Zijlema 2010) and include the coupled effects of waves and surge (Dietrich et al. 2011b, 2012a). These models have been validated extensively for storms impacting the Gulf coast, including Katrina and Rita (Bunya et al. 2010; Dietrich et al. 2010), Gustav (Dietrich et al. 2011a), and Ike (Hope et al. 2013). These high-resolution models are costlier per simulation, but have been shown to scale efficiently in high-performance computing environments (Tanaka et al. 2011). By using precomputed simulations from flood risk mapping studies (Irish et al. 2009; Kennedy et al. 2012; USACE 2015), recent studies have demonstrated their ability to provide probabilistic guidance (Taflanidis et al. 2013a, b).

Wave and surge models rely on atmospheric forcing, which is often simplified for efficiency in a forecasting application. Instead of using a high-fidelity, full-physics atmospheric model and/or assimilating meteorological observations, the surface pressure and wind fields are represented by using a simple vortex model, which can be developed from a small set of storm parameters in each forecast advisory (Schloemer 1954; Holland 1980). These parametric vortex models are cheap to construct and implement within existing wave and surge models, and can be applied immediately after each forecast advisory is issued (Xie et al. 2006; Gao et al. 2017). Recent advancements in high-resolution coupled model development and high-performance computing have made it possible for full-physics, dynamic prediction models to forecast storm structure and intensity with increased skill. Fully coupled, atmosphere-wave-ocean models produce better surface winds than uncoupled atmospheric models (Chen et al. 2013; Chen and Curcic 2016). However, there is limited predictability and large uncertainty in hurricane track and intensity in general (Judt et al. 2016).

As these systems make better use of high-performance computing and high-fidelity models, it is timely to investigate how the models can be coupled and then quantify their performance. The goals of this study are to quantify the relative performance of parametric vortex and full-physics atmospheric models, and their effects on predictions of storm surge and overland flooding, through hindcasts and forecasts of Hurricane Isaac (2012). The authors use a novel parametric vortex model with an improved representation of the pressure and wind fields, and compare it for the first time with a full-physics atmospheric model, which provides multiple, moving fields for surface pressures and wind velocities. The atmospheric conditions will be applied within tightly coupled wave and circulation models on a high-resolution, unstructured, finite-element mesh describing the coastal systems of southern Louisiana, Mississippi, and Alabama; this system has been validated extensively in this region. Model performance will be quantified via comparisons with observations at buoys and gauges of atmospheric pressures, wind velocities, and water levels.

Hurricane Isaac (2012)

Synoptic History

Isaac was weaker and slower moving than other storms that recently impacted the U.S. coastline along the Gulf of Mexico. The storm originated from a tropical wave off the coast of Africa on August 16, 2012, and moved westward in the Atlantic Ocean before entering the Caribbean Sea by August 23, 2012 (Berg 2013). It intensified to a maximum wind speed of 28 m s^{-1}, and its inner core organized enough to show hints of an eye. Isaac moved through the Caribbean Sea and passed over Hispaniola and Cuba, and then entered the Gulf of Mexico on August 27, 2012.

Although the storm was large, its intensification was suppressed partly due to disorganization of its inner core, so it did not achieve hurricane status until 1200 coordinated universal time (UTC) on August 28, 2012, or about 12 h before its initial landfall in Louisiana (Berg 2013). Isaac made landfall at 0000 UTC on August 29, 2012, near the western tip of the Mississippi River Delta, moved offshore near Barataria Bay, and then made a second landfall at 0800 UTC on August 29, 2012, near Port Fourchon, Louisiana. The rainfall was intense in southern Louisiana as the storm was making landfall, including rainfall totals of 52.4 cm in metropolitan New Orleans. These rainfall totals were enhanced by the storm's slow forward speed, and the storm's counterclockwise rotation pushed surge along the Louisiana-Mississippi continental shelf, including reports of a total water level of 3.4 m measured by a tide gauge near Shell Beach on Lake Borgne east of New Orleans. This storm surge threatened the hurricane and storm damage risk reduction system around New Orleans and caused extensive flooding in communities, such as Braithwaite and Laplace, Louisiana, which were located outside of the system.

Challenges for Forecasting

As Isaac moved from the Caribbean Sea toward the Gulf of Mexico, the storm interaction with the islands and changes in the large-scale environment may have contributed to the uncertainty in track forecasts by operational models. Most models and the National Hurricane Center (NHC) forecasts had a bias toward the Florida coast. In the advisories issued by the NHC, the storm's track was uncertain, especially as it moved westward through the Caribbean Sea. The predicted landfall location varied along the Florida coastline and then appeared to stabilize on the Florida panhandle near Pensacola, notably during NHC advisories 13–20 issued over 2 days from August 24 to 26, 2012. For NHC Advisory 13, when the storm center was located in the Caribbean Sea south of Hispaniola, the 5-day forecast put landfall to the west of Pensacola, but the cone of uncertainty extended more than 800 km from Vermilion Bay, Louisiana, through the entire Florida panhandle. By NHC Advisory 20, when the storm center had moved north of Cuba, the 3-day forecast put landfall to the east of Pensacola, and the cone of uncertainty had narrowed to 500 km from Alabama through Tallahassee, Florida. Thus, less than 72 h before Isaac's initial landfall, the forecast excluded Louisiana. The projected landfall location then shifted westward during August 26, 2012, and settled on southeastern Louisiana by NHC Advisory 24, which was issued at 0300 UTC on August 27, 2012.

These uncertainties about the forecast track and intensity created a wide range of possible outcomes for southeastern Louisiana. When Isaac was projected to make landfall along the Florida panhandle, the regions to the west (including Louisiana) would have experienced a relatively mild environment of offshore winds. After the projected track shifted westward, the storm was expected to intensify significantly, and southeastern Louisiana would have been subjected to stronger winds than actually occurred. These uncertainties in atmospheric conditions are passed forward to the forecasts of storm-induced waves and surge.

Models

Surface Pressures and Wind Velocities

Observation-Based Analysis Product

The first source of atmospheric forcing considered in this study is the real-time hurricane wind analysis system (HWind), which was

developed as part of the National Oceanic and Atmospheric Administration (NOAA) Hurricane Research Division (Powell et al. 1998). HWind incorporates observations of wind velocity relative to the storm center and converts them to a common reference frame at a 10-m height, a peak 1 min-averaged sustained wind speed, and marine exposure. Observations can include data from airborne stepped-frequency microwave radiometers, global positioning system (GPS) dropsondes, buoys, ships, satellite-based visual imagery, and land-based platforms (DiNapoli et al. 2012). These observations of wind velocities are then smoothed and interpolated onto a regular grid by minimizing the least-square differences between observations and analysis (Powell and Houston 1996). Through the 2012 hurricane season, these wind fields were produced and released in real-time as observations became available during a storm.

The HWind fields for Isaac are available from 1930 UTC on August 21, 2012, through 1930 UTC on August 29, 2012, or 8 days. The temporal resolution is at least every 6 h, but it is increased to 3 h during the peak of the storm. The wind velocities are provided on a regular grid with a spatial resolution of about 6 km, and the coverage is translated with the storm, so that the wind fields extend about 475 km in all four cardinal directions from the storm center. These winds first extended to southeast Louisiana at 1000 UTC on August 27, 2012, and the entire region was affected by 1800 UTC on August 27, 2012, with winds of 12 m/s or weaker. The winds increased in the region during the next 30 h before the initial landfall.

The ADvanced CIRCulation (ADCIRC) (Westerink et al. 2008) modeling system can read the HWind fields in their native file format, interpolate the wind velocities onto the ADCIRC unstructured mesh, and then use them as forcing for the waves and surge. The wind velocities are converted from a 1-min sustained wind speed to a 10-min wind speed for use by ADCIRC by using a multiplier of 0.893 (Powell and Houston 1996). The HWind fields do not include surface pressures, so the central pressures from the NHC best track (BT) guidance were used with a symmetric vortex model (Holland 1980) to generate pressure fields. The central pressure is specified at every HWind snap, and it is used with the maximum wind speed to compute a surface pressure at every computational point. These pressure and wind fields are based on observations, and were not available fully until after the storm.

Parametric Representation

The wind and pressure fields associated with tropical cyclones are often modeled using a parametric representation of a translating vortex. The most widely used parametric model was developed by Holland (1980) who solved the gradient wind equation assuming that the surface pressure profile can be approximated by a rectangular hyperbola (Schloemer 1954) with two scaling parameters. Values for the scaling parameters were determined by setting $V = V_{\max}$ and $dV/dr = 0$ at $r = R_{\max}$ and assuming a cyclostrophic balance (i.e., the Coriolis acceleration is negligible compared with the centrifugal acceleration) at $r = R_{\max}$ (Holland 1980). This model has been used for engineering design and storm surge modeling since its introduction, partly because it requires only a few storm parameters (i.e., central pressure, maximum wind velocity, radius to maximum wind velocity), which can be predicted with increasing skill during storm events. The Holland model has been used and extended for forecasting during several recent storms (Mattocks and Forbes 2008; Forbes et al. 2010), including a different radial profile in each storm quadrant to improve the representation of storm asymmetry (Xie et al. 2006). Hu et al. (2012) improved on the Holland model formulation by removing the cyclostrophic balance assumption and by introducing a piecewise continuous radial wind profile that matched multiple specified wind isotachs in each quadrant of the storm. However, they used only a single scaling parameter in the pressure profile and were limited to satisfying only $V = V_{\max}$ at $r = R_{\max}$. Thus, their formulation does not force an actual maximum in the radial wind profile at $V = V_{\max}$.

In this study, the authors use the recently developed generalized asymmetric Holland model (GAHM) (Gao et al. 2017), which includes the previous improvements (Xie et al. 2006; Hu et al. 2012, 2015), but reintroduces the two scaling parameters from the original Holland formulation, satisfying both $V = V_{\max}$ and $dV/dr = 0$ at $r = R_{\max}$ without assuming a cyclostrophic balance at $r = R_{\max}$. The cyclostrophic balance is violated by large and weak storms, which is often typical of storms as they approach landfall (Hu et al. 2012; Gao et al. 2017).

The resulting equations for GAHM are, for the surface pressure field

$$P(r) = P_c + (P_n - P_c)e^{-\psi(R_{\max}/r)^{B_g}} \tag{1}$$

and for the gradient wind profile

$$V_g(r) = \sqrt{V_{\max}^2(1 + 1/R_o)e^{\psi\left(1-(R_{\max}/r)^{B_g}\right)}(R_{\max}/r)^{B_g} + \left(\frac{rf}{2}\right)^2} - \left(\frac{rf}{2}\right) \tag{2}$$

where P and V_g = surface pressure and gradient wind speed at radius r; P_c = central pressure; P_n = ambient background pressure; $R_{\max}$ = radius to maximum winds; $R_o = R_{\max}/f\,V_{\max}$ = Rossby number; and f = Coriolis parameter. The generalized Holland parameter B_g and an intermediate factor ψ are given by

$$B_g = B\frac{(1 + 1/R_o)e^{\psi-1}}{\psi} \qquad \psi = 1 + \frac{1/R_o}{B_g(1 + 1/R_o)} \tag{3}$$

where $B = V_{\max}^2\rho e/(P_n - P_c)$ = original Holland B. These equations are solved iteratively within ADCIRC.

As noted previously, this formulation ensures that both

$$V(r = R_{\max}) = V_{\max} \qquad \frac{dV}{dr}(r = R_{\max}) = 0 \tag{4}$$

providing a smooth wind field through the $R_{\max}$. Without the criterion on $d\,V/dr$, the maximum wind speed does not necessarily occur at $r = R_{\max}$. With this improvement, GAHM is a better representation of the storm described in the forecast advisories, and this study is the first instance in which its performance will be compared with full-physics atmospheric models.

GAHM has been implemented within ADCIRC, so the surface pressure and wind fields can be determined dynamically at every point in the computational domain. When applied within the ADCIRC surge guidance system (ASGS) (Fleming et al. 2008; Blanton et al. 2012; Dresback et al. 2013), this process is automated during every forecast advisory. When each new advisory is issued by the NHC, the ASGS pulls the storm parameters to perform nowcast and forecast simulations. This process is repeated for each advisory during the storm, and guidance products are shared with emergency management partners in local, state, and federal agencies. It is noted that, although GAHM has been applied to other storms (Gao et al. 2017; Cyriac et al. 2017), and was used during the 2015

and subsequent hurricane seasons, it was not available for Isaac in 2012. The GAHM results presented in this paper were obtained by using the same advisories issued during the storm; thus, they represent forecast guidance.

Fully Coupled Atmosphere-Wave-Ocean Prediction

The unified wave interface (UWIN) is a generalized air-sea interface coupler that is designed to be flexible in a multimodel system and portable for transition to the next-generation, fully coupled, regional and global atmosphere-wave-ocean-land models. UWIN has been implemented in the coupled model (UWIN-CM) (Chen and Curcic 2016), which consists of the atmosphere, wave, and ocean model components and coupling based on methods described in Chen et al. (2007) and Chen et al. (2013).

The atmospheric model in UWIN-CM is the weather research and forecasting (WRF) model with advanced research WRF dynamic core (Skamarock et al. 2008). WRF is a nonhydrostatic atmospheric model with a large number of model physics options and a storm-following, moving-nest capability for hurricane forecasting. The outermost domain is from 55.0°W to 103.0°W in longitude and 7.0°N to 45.0°N in latitude with 12-km horizontal grid spacing and 36 vertical levels. There are two vortex-following inner nests of 2,000 × 2,000 km^2 and 440 × 440 km^2 with 4- and 1.3-km grid spacing, respectively. The ocean surface wave model in UWIN-CM is the University of Miami wave model (UMWM) (Donelan et al. 2012). The wave model has the same domain as the WRF outer domain, and it is configured with 4-km grid spacing in this study. The wave energy spectrum is represented by 36 directional bins and 37 frequency bins ranging from 0.0313 to 2.0 Hz. The ocean circulation model in UWIN-CM is the hybrid coordinate ocean model (HYCOM) (Wallcraft et al. 2009). HYCOM domain covers the region of the WRF outer domain. It is configured with 0.04° horizontal mesh spacing (varying from about 3.8 to 4.4 km from the north-south of the model domain) and 32 vertical levels.

UWIN handles the coupling between model components. It contains the coupling physics and a common exchange mesh that is used for interpolation and calculation of air-sea exchange fields from the component models. The WRF model initial and lateral boundary conditions were from the real-time global forecasting system (GFS) 6 hourly forecast fields at a 0.5° horizontal resolution. The initial and boundary conditions for the ocean model are provided by the global, data-assimilated, 0.08° horizontal resolution daily HYCOM fields. The UWIN-CM forecasts of Hurricane Isaac were initialized at 1200 UTC on August 26 and 27, 2012.

The surface wind and pressure fields from UWIN-CM are saved in compressed output files. The ADCIRC modeling system was extended in this study to read these gridded fields in the NetCDF format, consider fields on three domains (i.e., the outermost domain with 12-km resolution, and two inner nests with 4- and 1.3-km resolution), and to recompute the interpolation weights onto the ADCIRC unstructured mesh as the inner nests follow the storm center. This code extension allows for the UWIN-CM fields to be read and used directly by the ADCIRC modeling system, and it represents the first instance that the system has received atmospheric forcing in this fashion.

Waves and Storm Surge

The coastal ocean response to the atmospheric forcing of Isaac is modeled with the simulating waves nearshore (SWAN) and ADCIRC models. These models are coupled tightly as one executable program, so they pass information through local memory and are highly efficient in parallel computing environments. These models have been applied successfully to detailed hindcasts of several recent storms in the Gulf of Mexico, including Katrina and Rita (Dietrich et al. 2011b), Gustav (Dietrich et al. 2011a), and Ike (Hope et al. 2013).

Tight Coupling of SWAN + ADCIRC

SWAN represents the wave field as a phase-averaged spectrum (Booij et al. 1999; Ris et al. 1999). The wave action density $N(t, \lambda, \varphi, \sigma, \theta)$ evolves in time (t), geographic space (with longitudes λ and latitudes φ), and spectral space (with relative frequencies σ and directions θ), as governed by the action balance equation. Source terms represent wave growth by wind; energy lost due to whitecapping, depth-induced breaking, and bottom friction; and energy exchanged between spectral components due to nonlinear effects in deep and shallow water. Wind input is based on the formulation from Cavaleri and Malanotte-Rizzoli (1981) and Snyder et al. (1981), whitecapping is applied via the expression of Komen et al. (1984) as modified by Rogers et al. (2003), and nonlinear quadruplet interactions are computed using the discrete interaction approximation of Hasselmann et al. (1985). Bottom friction is parameterized via the conversion of spatially variable Manning's n values into roughness lengths (Bretschneider et al. 1986; Madsen et al. 1988; Dietrich et al. 2011a), whereas depth-induced breaking is computed with a spectral version of the model due to Battjes and Janssen (1978) with the breaking index $\gamma = 0.73$. Nonlinear triad interactions are neglected. Excessive refraction and frequency shifting are limited via Dietrich et al. (2013). The wave directions are discretized into 36 directional bins of constant width 10°, and the frequencies are discretized over 40 bins on a logarithmic scale over the range of 0.031–1.42 Hz.

ADCIRC solves modified forms of the shallow-water equations (SWEs) for water levels ζ and depth-averaged currents $\vec{U}$ (Kolar et al. 1994; Luettich and Westerink 2004; Dawson et al. 2006; Westerink et al. 2008). Water levels are computed via the solution of the generalized wave continuity equation (Kinnmark 1986), whereas currents are obtained from the vertically integrated momentum equations. ADCIRC uses the continuous-Galerkin finite-element method with linear C_0 triangular elements to discretize and solve the modified SWE on unstructured meshes, allowing localized refinement in regions in which the solution gradients are largest. Bottom friction is specified via spatially variable Manning's n values based on land-use/land-cover datasets (Dietrich et al. 2011a). A vertical datum correction of 0.134 m is added to the water levels to convert to NAVD88 (2004.65) (Bunya et al. 2010), and constant flow rates are specified at the Mississippi and Atchafalaya Rivers.

SWAN can use unstructured meshes (Zijlema 2010), and the SWAN + ADCIRC models were coupled tightly to run as the same executable program (Dietrich et al. 2011b). The models use the same unstructured mesh, both globally and locally in a parallel computing environment, so it is not necessary to interpolate information between heterogeneous meshes. The tight coupling of SWAN + ADCIRC has been validated for several recent storms impacting the Louisiana coastline (Dietrich et al. 2012a). The models alternate running on the same computational core; in this paper, the coupling interval and SWAN time step are taken to be 1,200 s, and the ADCIRC time step is 1 s. The source codes and input and output files have been archived so the following simulations are repeatable (Dietrich et al. 2017a, b, c).

Input of Atmospheric Forcing

Atmospheric forcing is the primary driver of waves and circulation during storm events. For SWAN, the wind input uses a linear

component based on the formulation from Cavaleri and Malanotte-Rizzoli (1981) and Snyder et al. (1981), as well as an exponential component from Komen et al. (1984). These components depend on the friction velocity U_*, which depends on the wind speed U_{10} at a 10-m elevation

$$U_*^2 = C_D \, U_{10}^2$$

where C_D = drag coefficient and is expressed typically as a function of the wind speed U_{10}.

ADCIRC uses the wind speeds U_{10} to compute its surface stresses τ^s

$$\frac{\tau^s}{\rho} = C_D \, U_{10}^2$$

where ρ = reference air density. The drag coefficient formulation has also evolved in ADCIRC, starting with the linear

Table 1. Summary of Geographic Locations Shown in Fig. 1

Type	Label	Location
Cities	A	New Orleans, Louisiana
	B	Port Fourchon, Louisiana
	C	Biloxi, Mississippi
Water bodies	D	Lake Pontchartrain
	E	Barataria Bay
	F	Bay St. Louis
Channels	G	Gulf Intracoastal Waterway
	H	Mississippi River Gulf Outlet
	I	Mississippi River Delta
Barrier Islands	J	Chandeleur Islands
	K	Grand Isle
Overland regions	L	Biloxi Marsh
	M	Caernarvon Marsh
	N	Plaquemines Parish

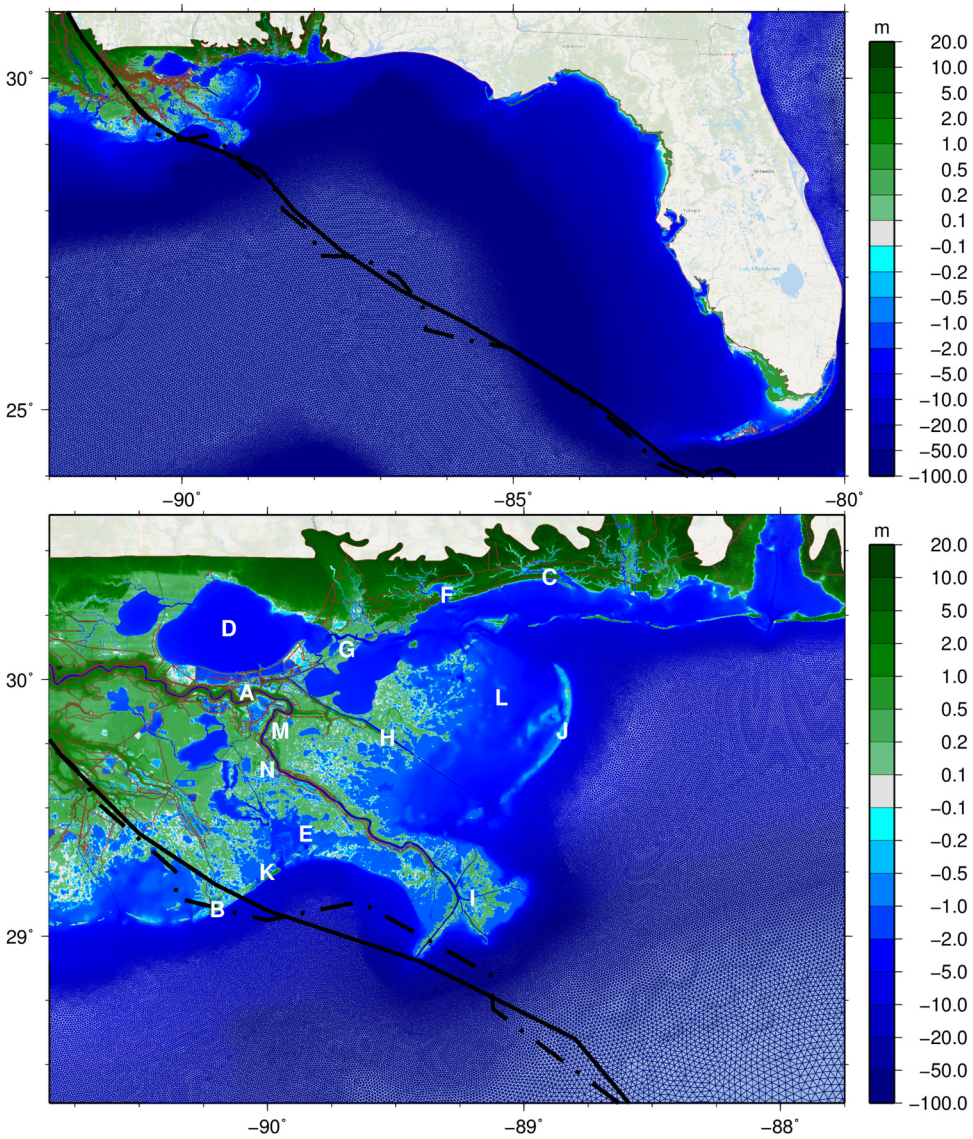

Fig. 1. (Color) Bathymetry and topography (meters relative to mean sea level) in the SL16 unstructured mesh for the northern Gulf coastline; geographic locations of interest are indicated by letters identified in Table 1 [Note: Storm tracks for HWind (dot-dashed) and GAHM-BT (solid) are indicated]

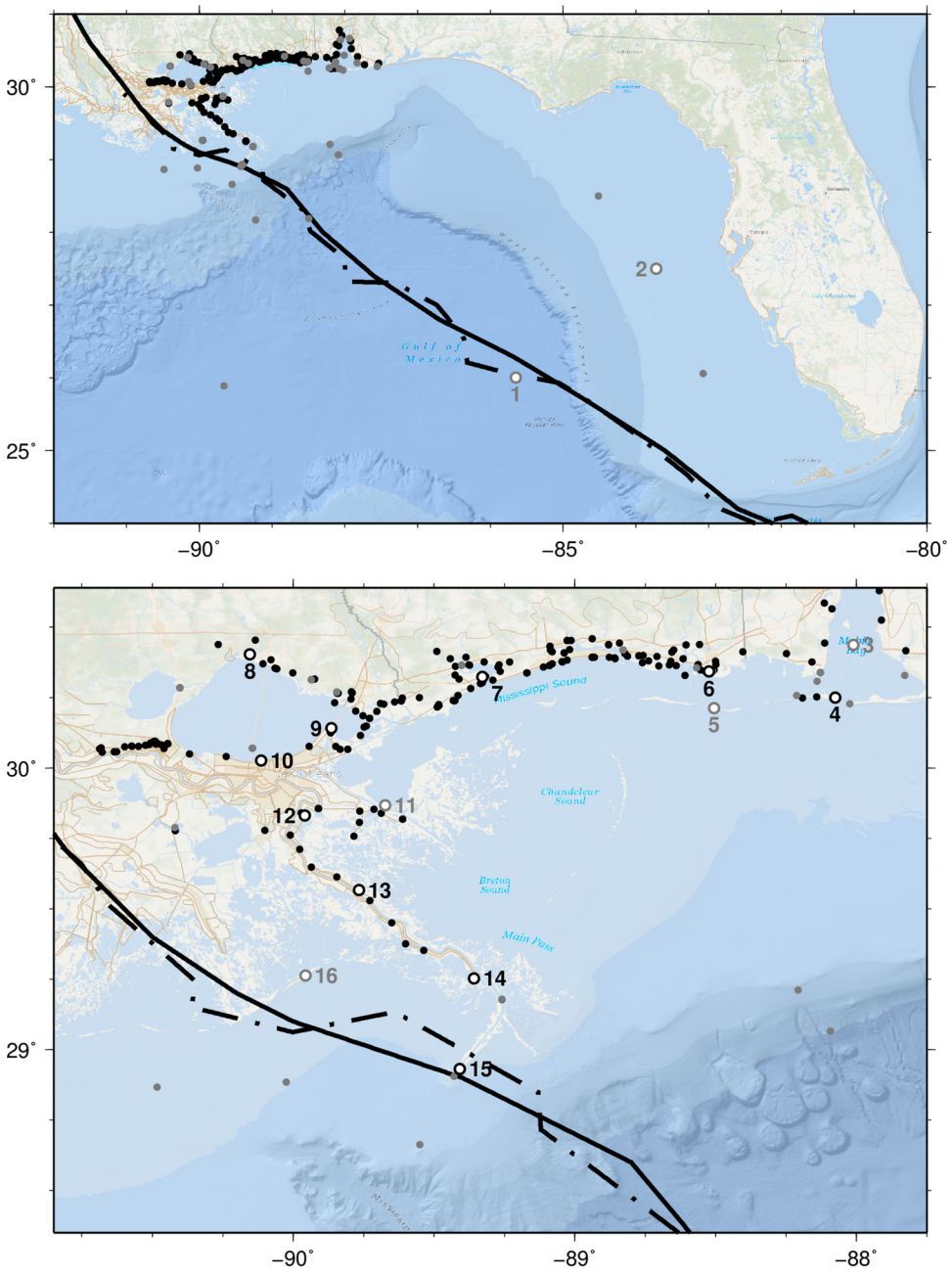

Fig. 2. (Color) Locations of meteorological (gray dots) and water level (black dots) observations during Isaac at buoys and gauges operated by the NDBC, DISL, NOS, USGS, and other entities; the numbered stations are described in Table 2; their observations were used for analyses in Figs. 3 and 4 [Note: Storm tracks for HWind (dot-dashed) and GAHM-BT (solid) are indicated]

expression from (Garratt 1977), and now using a sector-based formulation in which the drag coefficient also depends on the location relative to the eye of the storm (Powell 2006; Black et al. 2007; Dietrich et al. 2011a). In the coupling of SWAN + ADCIRC, this drag coefficient is shared between both models, overriding the default setting in SWAN. In addition to the surface stresses, ADCIRC also considers the inverted barometer effect due to surface pressures. Thus, for a storm simulation, the SWAN + ADCIRC models require temporally and spatially variable inputs of atmospheric pressures and wind speeds throughout the computational domain.

SL16 Unstructured Mesh

Isaac's impact on the surge conditions in southeastern Louisiana are simulated by SWAN + ADCIRC using the SL16 unstructured, finite-element mesh (Fig. 1). The SL16 mesh was developed for studies of hurricane-induced flooding in this region (Dietrich et al. 2011a, 2012a; Martyr et al. 2013; Kerr et al. 2013), and has been used in a study of oil spill transport following the Deepwater Horizon event (Dietrich et al. 2012b). The mesh has coverage of the entire Gulf of Mexico and Caribbean Sea, as well as the western North Atlantic Ocean, to allow storms to develop within its domain.

However, most of the mesh resolution is concentrated within the low-lying regions of southeastern Louisiana, Mississippi, and Alabama. Mesh spacings vary from 4 to 6 km in the deeper Gulf, to less than 1 km on the continental shelf, to less than 200 m in the wave-breaking zones and inland regions, to as small as 20 m in the natural and manufactured channels that connect through the intricate system of marshes and bayous surrounding New Orleans. Waves and surge are allowed to develop in deep water and on the continental shelf, respectively, and then propagate into and dissipate within the complex nearshore environment.

Bathymetric depths and topographic elevations were mapped onto the SL16 mesh from available high-resolution data sets, and input conditions were developed for Manning's *n* roughness coefficients, directional wind adjustment factors, and other spatially variable parameters; this mesh development is described in Dietrich et al. (2011a). Although newer meshes have evolved recently by extending high-resolution coverage into adjoining regions, most notably for a study of the far-reaching impacts of Ike (2008) throughout Louisiana and Texas (Hope et al. 2013), the SL16 mesh remains the highest resolution representation of southeastern Louisiana.

Results

In the sections that follow, the performance of ADCIRC in predicting storm surge and coastal flooding is evaluated with three sources of atmospheric forcing, and for both hindcasts and forecasts. First, the model is applied to hindcasts using the HWind analysis product and GAHM with NHC BT guidance. It is shown that the water-level predictions with GAHM forcing are a better match to observations of hydrographs and high-water marks (HWMs) throughout southeastern Louisiana, Mississippi, and Alabama. Then, the model is applied to forecasts using GAHM with NHC advisories released during the storm. It is shown that the surge hazard was changed significantly in the 24 h when the predicted storm track was shifted from the Florida panhandle into Louisiana. Finally, the model is applied to forecasts using GAHM (with NHC advisory forecast tracks) and UWIN-CM for two advisories before and after the shift in storm track. It is shown that the UWIN-CM predicted track is better than the NHC advisory track at the long lead time in this case, and its wind field and associated ocean response are a closer match to the smaller scale wind and surge hazards.

Hindcasts Using HWind and GAHM with NHC BT Guidance

The authors examine the ADCIRC hindcasts of total water levels during Isaac, first by using hindcasts with atmospheric forcing that did not become available until after the event. The wind fields from HWind are used as atmospheric forcing to an ADCIRC simulation from 1930 UTC on August 21, 2012 through 1930 UTC on August 29, 2012, or a total of 8 days. The BT estimate issued poststorm by the NHC was used in GAHM to develop atmospheric forcing to an ADCIRC simulation from 0000 UTC on August 26, 2012, through 0000 UTC on August 31, 2012, or a total of 5 days. These simulations are denoted as HWind and GAHM-BT, respectively. In both simulations, the storm follows a track from southwest to northeast through the Gulf of Mexico, making an initial landfall in Louisiana at the Mississippi River Delta, and then a second landfall near Port Fourchon (geographic locations are identified in Fig. 1 and Table 1). It is noted that the BT estimate can be considered as an observed track for the storm; thus, model simulations using the BT should have minimal track error.

The wind and surge hazards were observed throughout the impacted region of the northern Gulf of Mexico (Fig. 2). A total of 40 stations are available to describe the wind hazards, including buoys and gauges operated by the National Data Buoy Center (NDBC), the Dauphin Island Sea Lab (DISL), the National Ocean Service (NOS), USGS, Shell Oil, the Louisiana Offshore Oil Port, and the Louisiana State University Coastal Studies Institute. A total of 146 stations are available to describe the surge hazards, including gauges operated by the NOS and USGS. Of these 146 hydrographs, 34 are discarded due to inconsistencies in the vertical datum, noise in the observed signal, or because the peak value was associated with rainfall runoff (which is not considered in this paper). The remaining 112 hydrographs describe the development of storm surge throughout Louisiana, Mississippi, and Alabama (Fig. 2).

Eight meteorological stations, with locations spanning from deep water to the northern Gulf coastline (Fig. 2 and Table 2), were selected to illustrate the wind hazards (Fig. 3). The deepwater buoys show the passage of the storm in the central Gulf, including at buoy 42003, at which the minimum pressure was 986 hPa and the maximum wind speed was 22 m s^{-1}. The evolution of the wind field was observed at stations along the coastlines of Alabama (at the DISL Middle Bay Lighthouse), Mississippi (at NOS station 8741003), and Louisiana (at NOS stations 8761305 and 8761927), at which the wind hazards were relatively small, with minimum pressures of 1,000 hPa and maximum wind speeds of 20–21 m s^{-1}. To the west of the Mississippi River, the gauges captured the strength of the storm as it made landfall (Fig. 3). At NOS station 8760922 in the delta, the minimum pressure was 971 hPa and the maximum wind speed was 33 m s^{-1}, with a double peak corresponding to the passage of the eye of the storm. At NOS station 8761724 on Grand Isle, the maximum wind speed was also greater than 30 m s^{-1}, but the winds decreased after landfall to 12–16 m s^{-1}.

Twelve stations located throughout the region (Fig. 2 and Table 2) are selected for analysis (Fig. 4). Along the Mississippi and Alabama coastlines, the observed peaks in the water levels

Table 2. Summary of Buoys and Gauges with Observations Used in the Analyses in Figs. 3 and 4, Including Whether Records Exist for Meteorology, Water Levels, or Both

Station number	Location	Station	Longitude	Latitude	MET	WL
1	GOM	NDBC 42003	–85.648	26.007	X	
2	GOM	NDBC 42022	–83.721	27.499	X	—
3	AL	DISL MBLA	–88.011	30.437	X	—
4	AL	NOS 8735180	–88.075	30.250	—	X
5	MS	NOS 8741003	–88.505	30.213	X	—
6	MS	USGS MS-JAC-033	–88.523	30.343	—	X
7	MS	USGS MS-HAN-013	–89.328	30.324	—	X
8	LA	USGS 302415090091465	–90.154	30.404	—	X
9	LA	USGS 300830089515000	–89.864	30.142	—	X
10	LA	NOS 8761927	–90.113	30.027	X	X
11	LA	NOS 8761305	–89.673	29.868	X	X
12	LA	USGS LA-PLA-019	–89.959	29.832	—	X
13	LA	USGS LA-PLA-004	–89.766	29.567	—	X
14	LA	USGS LA-PLA-010	–89.358	29.252	—	X
15	LA	NOS 8760922	-89.408	28.932	X	X
16	LA	NOS 8761724	-89.957	29.263	X	X

Note: AL = Alabama; GOM = Gulf of Mexico; LA = Louisiana; MS = Mississippi; MET = meteorology; WL = water levels; locations are also shown in Fig. 2.

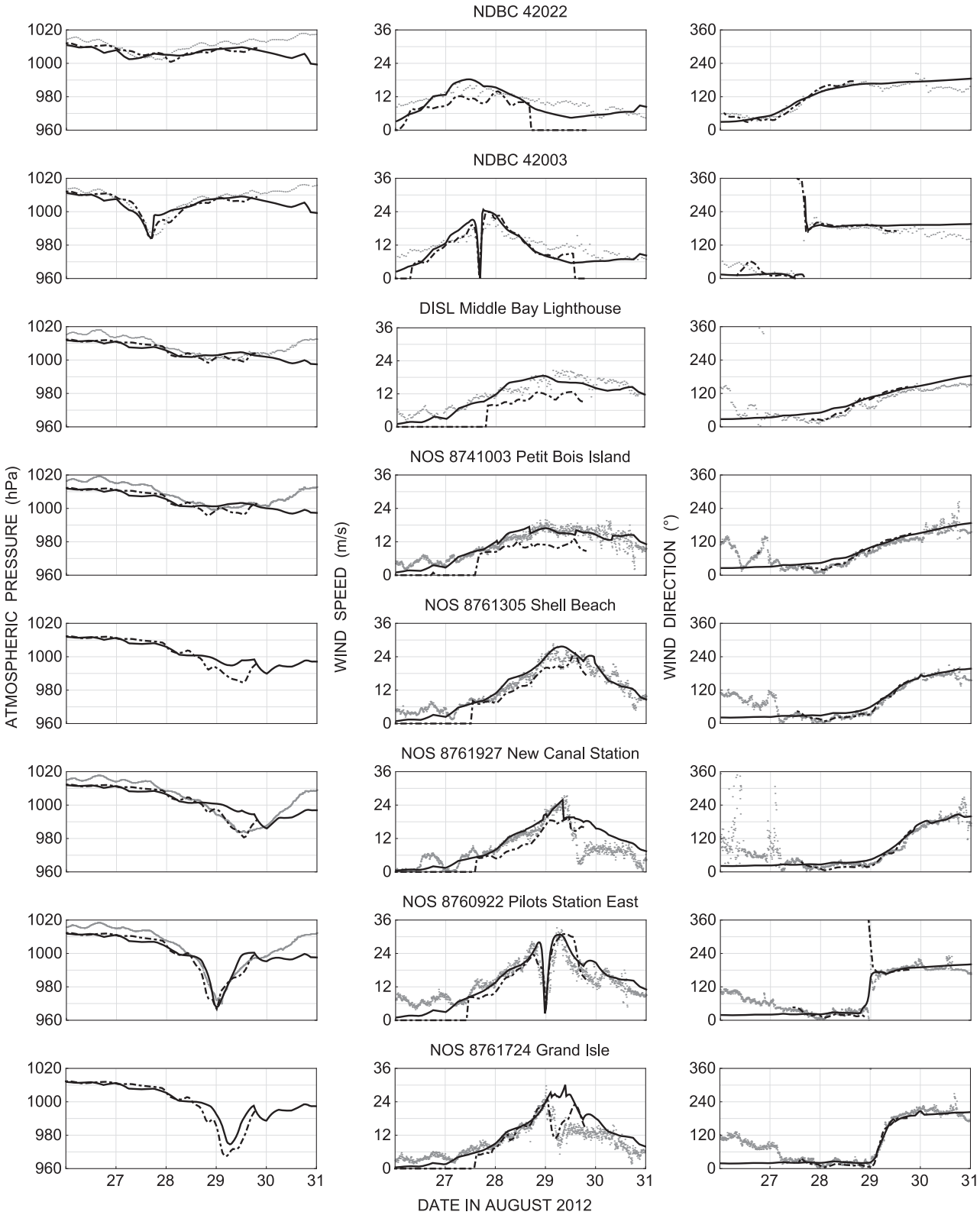

Fig. 3. Time series of atmospheric pressures (hPa), wind speeds (m s^{-1}), and wind directions (degrees clockwise from true north) in the left, center, and right columns, respectively, at eight selected stations with locations described in Table 2 and shown in Fig. 2 [Note: Subfigure lines indicate observations (gray) and hindcast simulations using atmospheric forcing from HWind (dot-dashed) and GAHM-BT (solid)]; atmospheric pressures were not measured at NOS stations 8761305 and 8761724

increased from east to west, from 1 m near Mobile Bay, to 2.5 m near Bay St. Louis. Within Lake Pontchartrain, the observed water levels showed a gradual increase in surge during the storm, with observed peaks between 2 and 2.5 m. These peaks occurred in the early hours of August 30, 2012, or about 16 h after Isaac's second landfall. In the Caernarvon and Biloxi marshes to the southeast of metropolitan New Orleans, the winds were easterly as the storm was making landfall, and they pushed surge from the shelf and against the levee systems along the Mississippi River, Mississippi River Gulf Outlet, and Gulf Intracoastal Waterway. The observations show the increase in peak water level, from 2 m near Pilottown and the open Gulf, to 4 m along the river levees at the edge of the marsh and near English Turn.

HWind underpredicts the wind speeds and water levels in southern Louisiana (Figs. 3 and 4). At deepwater NDBC buoys 42022 and 42003, the wind models perform well, with close matches to the timing and magnitude of the atmospheric pressures, as well as to the change in wind directions as the storm passed. However, HWind underpredicts the wind speeds by 3–4 m s^{-1} at buoy 42022, and both simulations show an incorrect double peak in the wind speeds at buoy 42003, which is likely due to their tracks being too close to this location. In Alabama, Mississippi, and Louisiana near New Orleans, GAHM-BT shows a close match to the peak wind speed, but HWind is low by 5–6 m s^{-1}. To the west of the river, both atmospheric forcings show a better match to the wind speeds, although GAHM-BT has an overprediction of 10–12 m s^{-1} as the

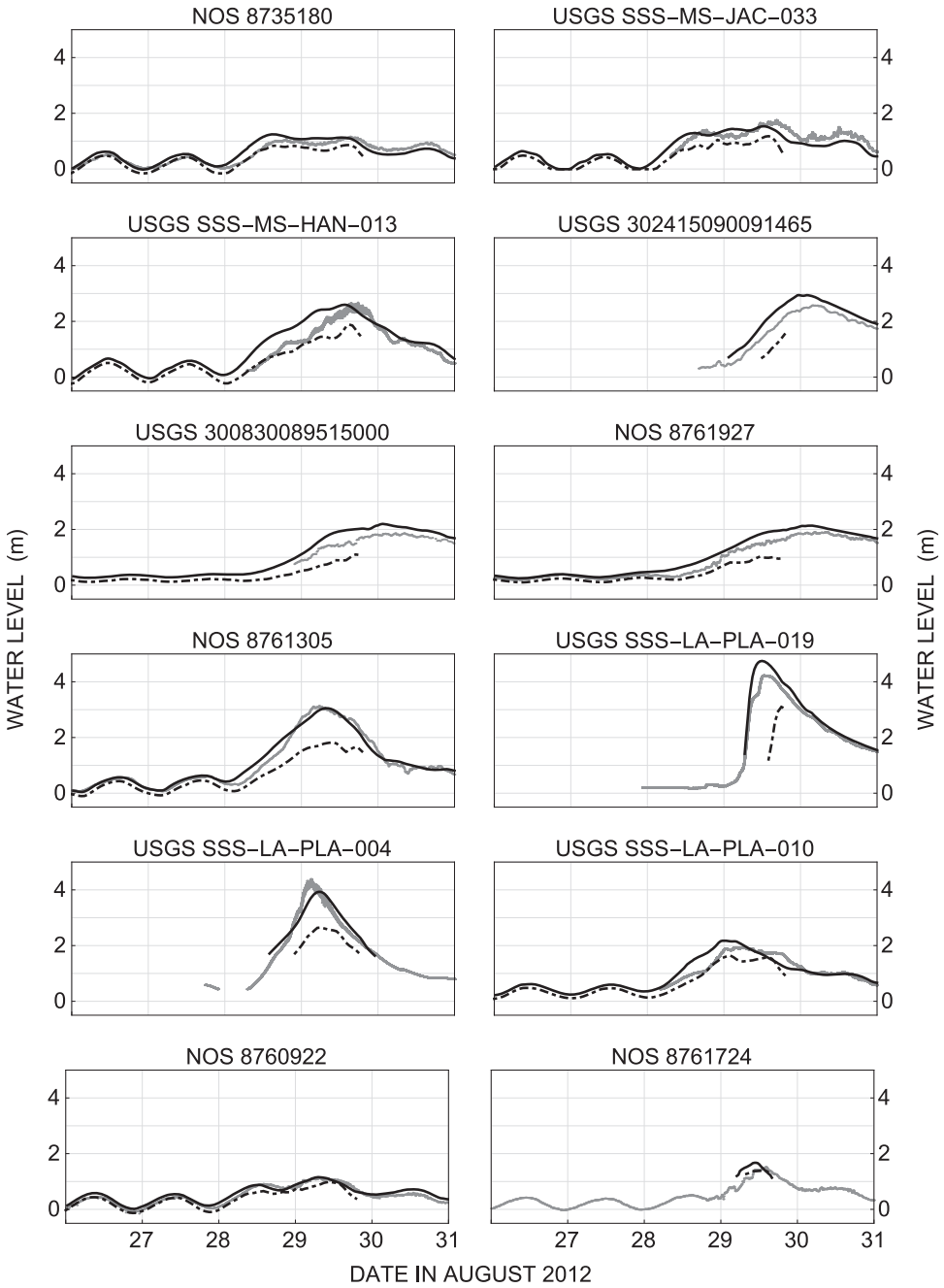

Fig. 4. Time series of water levels (meters relative to NAVD88) at 12 selected stations with locations described in Table 2 and shown in Fig. 2 [Note: Subfigure lines indicate observations (gray) and hindcast simulations using atmospheric forcing from HWind (dot-dashed) and GAHM-BT (solid)]

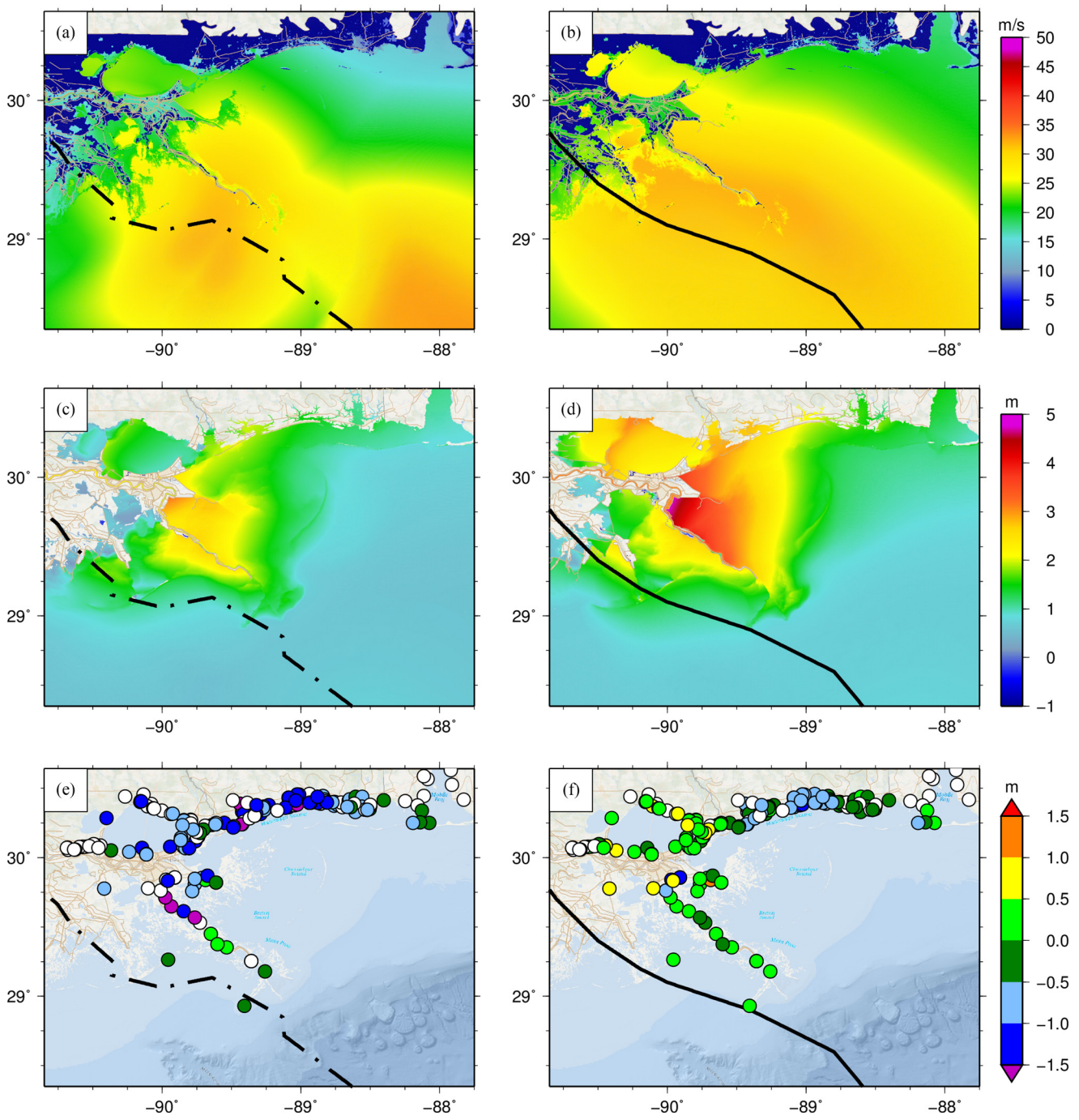

Fig. 5. (Color) Contours of maximum (a and b) wind speeds (m s^{-1}) and (c and d) water levels (meters relative to NAVD88) during Isaac indicate locations (e and f) of the hydrographs and HWMs; the points are color coded to show the errors between measured and modeled peak water levels [Note: Orange, yellow, and light green circles indicate overprediction by the model; green, blue, dark blue, and purple circles indicate underpredictions; white circles indicate locations that were never wetted by ADCIRC; the left column shows results from HWind (dot-dashed), and the right column shows results from GAHM-BT (solid)]

storm was making its second landfall near Port Fourchon. The differences between HWind and GAHM-BT are due mostly to the differences in wind structure, because their tracks are similar. These trends in the atmospheric forcing are then translated into the water-level predictions (Fig. 4). In Alabama and Mississippi, the HWind water levels are too low by about 0.5 m during the peak of the storm. This underprediction is increased to about 1 m at the gauges in Louisiana near New Orleans, and more than 2 m at the gauges in the Caernarvon Marsh. GAHM-BT shows close matches to the hydrographs, including within 0.5 m to the peak values.

The maximum wind speeds are similar for both HWind and GAHM-BT, with peaks of about 35 m s^{-1} to the northeast of the storm track [Figs. 5(a–d)]. HWind shows a variation in the storm intensity as it made landfall, with a decrease in maximum wind speeds as the storm approached the Mississippi River Delta, an increase as the storm moved south of Barataria Bay toward Port Fourchon, and then another decrease after its second landfall. GAHM-BT shows a

steadier wind field; its storm track is straighter, and the maximum wind speeds are relatively constant as the storm makes landfall. The GAHM-BT wind fields thus affect a larger area, with maximum wind speeds greater than 25 m s^{-1} throughout Louisiana, and maximum wind speeds of about 20 m s^{-1} along the Mississippi-Alabama coasts. This broader wind field causes the maximum water levels to be higher for GAHM-BT. Whereas HWind shows a peak water level of about 3 m at the top of Caernarvon Marsh and less than 2 m inside Lake Pontchartrain, GAHM-BT shows peaks that are higher by about 1 m throughout Louisiana.

To quantify these errors, the model predictions are compared with the observations by using statistical error measures, including the mean normalized bias (B_{MN}, which is a measure of the model's magnitude of overprediction or underprediction normalized to the observed value, with an ideal value of zero)

$$B_{MN} = \frac{\frac{1}{N}\sum_{i=1}^{N} E_i}{\frac{1}{N}\sum_{i=1}^{N} |O_i|}$$

and RMS error (E_{RMS}, which is a measure of the magnitude of the error, with an ideal value of zero)

$$E_{RMS} = \sqrt{\frac{1}{N}\sum_{i=1}^{N} E_i^2}$$

where O = observed value; E = error in terms of modeled minus observed; and N = number of observations. These error measures are computed for the atmospheric pressures, wind speeds, and water levels and are summarized in Tables 3 and 4. HWind and GAHM-BT are similar in their performance when compared with the observations. The RMS errors for atmospheric pressures are smaller for HWind (about 3.7 hPa) compared with GAHM-BT (about 6 hPa), but this difference is reversed for the wind speeds, for which GAHM-BT shows smaller errors by 0.3–0.7 m/s^{-1}. The behavior is not different significantly for the full set of 40 stations compared with the subset of 8 stations.

For the water levels, HWind shows a negative bias, indicating that it is underpredicting the peak water levels during the storm, whereas GAHM-BT shows a slightly positive bias. The RMS errors are about 0.54–0.61 m for HWind, but about 0.27–0.35 m for GAHM-BT. These trends are also evident in the spatial distribution of model performance for HWMs and peak water levels [Figs. 5(e and f)]. The HWind errors are shown in shades of blue at many of the stations in the region, indicating an underprediction of the peak values, whereas the GAHM-BT errors are shown to be within 0.5 m at most of the stations. When plotted as a one-to-one comparison between observed and modeled peak values (Fig. 6), HWind has an average error of –0.87 m and a best fit slope of 0.64, whereas GAHM-BT has an average error of –0.10 m and a best fit slope of 0.94.

Thus, GAHM-BT is a better representation of the atmospheric forcing and associated ocean response during Hurricane Isaac. It is a better match to the observed time series of wind speeds and water levels, and to the peak water levels, at locations throughout the region. It is noted that this finding will not be necessarily true for other storms and other regions, because generally the data-

Table 4. Summary of Error Statistics for the Water Levels

		Water levels	
Model	Stations	B_{MN}	E_{RMS} (m)
HWind	112	$-3.16.10^{-1}$	$6.06.10^{-1}$
	12	$-2.87.10^{-1}$	$5.38.10^{-1}$
GAHM-BT	112	$8.38.10^{-2}$	$3.45.10^{-1}$
	12	$1.17.10^{-1}$	$2.73.10^{-1}$
GAHM-21	112	$-7.97.10^{-1}$	$1.32.10^{\circ}$
	12	$-7.21.10^{-1}$	$9.43.10^{-1}$
GAHM-25	112	$-7.29.10^{-2}$	$4.90.10^{-1}$
	12	$-1.11.10^{-1}$	$4.21.10^{-1}$
UWIN-CM-21a	112	$1.62.10^{-1}$	$5.54.10^{-1}$
	12	$1.73.10^{-1}$	$4.76.10^{-1}$
UWIN-CM-25a	112	$2.85.10^{-2}$	$4.16.10^{-1}$
	12	$-1.13.10^{-2}$	$4.55.10^{-1}$
UWIN-CM-25a+6h	112	$2.99.10^{-4}$	$2.55.10^{-1}$
	12	$-2.95.10^{-2}$	$2.02.10^{-1}$

Note: Values are given for the 112 water-level observation stations with locations shown in Fig. 2, as well as for the subset of 12 stations with time series behavior shown in Fig. 4.

Table 3. Summary of Error Statistics for the Atmospheric Pressures and Wind Speeds

		Atmospheric pressures		Wind speeds	
Model	Stations	B_{MN}	E_{RMS} (hPa)	B_{MN}	E_{RMS} (m s^{-1})
HWind	40	$-2.79.10^{-3}$	$3.70.10^{0}$	$-1.40.10^{-1}$	$4.58.10^{0}$
	8	$-2.61.10^{-3}$	$3.61.10^{0}$	$-1.56.10^{-1}$	$4.16.10^{0}$
GAHM-BT	40	$3.45.10^{-3}$	$6.17.10^{0}$	$1.01.10^{-1}$	$4.28.10^{0}$
	8	$-3.58.10^{-3}$	$6.06.10^{0}$	$2.06.10^{-2}$	$3.45.10^{0}$
GAHM-21	40	$-5.94.10^{-4}$	$1.40.10^{1}$	$-6.59.10^{-2}$	$5.43.10^{0}$
	8	$-5.42.10^{-3}$	$1.44.10^{1}$	$-1.45.10^{-1}$	$4.95.10^{0}$
GAHM-25	40	$3.65.10^{-3}$	$1.14.10^{1}$	$1.12.10^{-1}$	$4.31.10^{0}$
	8	$-4.99.10^{-3}$	$1.16.10^{1}$	$1.52.10^{-2}$	$4.02.10^{0}$
UWIN-CM-21a	40	$2.05.10^{-2}$	$3.69.10^{0}$	$1.22.10^{-1}$	$4.51.10^{0}$
	8	$-3.74.10^{-4}$	$3.32.10^{0}$	$1.16.10^{-1}$	$4.44.10^{0}$
UWIN-CM-25a	40	$1.62.10^{-2}$	$2.35.10^{0}$	$8.85.10^{-2}$	$3.93.10^{0}$
	8	$1.22.10^{-3}$	$2.76.10^{0}$	$3.69.10^{-2}$	$3.81.10^{0}$
UWIN-CM-25a+6h	40	$1.68.10^{-2}$	$3.05.10^{0}$	$6.98.10^{-2}$	$4.17.10^{0}$
	8	$6.11.10^{-4}$	$2.54.10^{0}$	$6.04.10^{-2}$	$3.78.10^{0}$

Note: Values are given for the 40 meteorological observation stations with locations shown in Fig. 2, as well as for the subset of eight stations with time series behavior shown in Fig. 3.

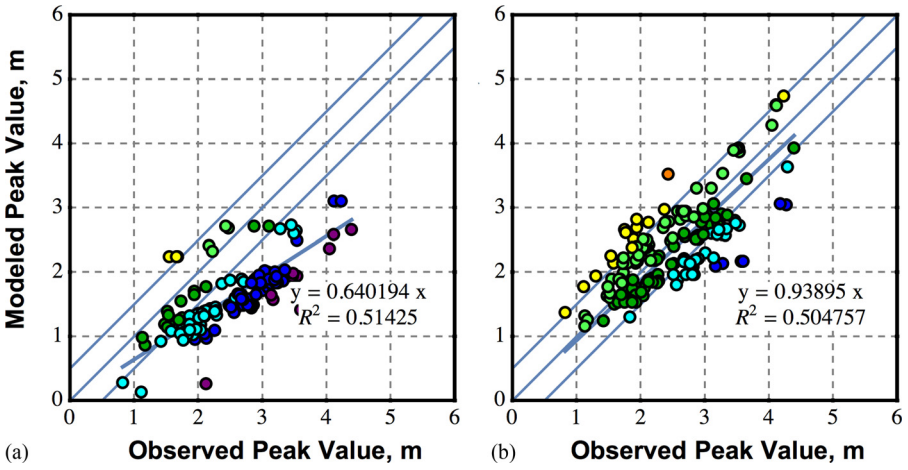

Fig. 6. (Color) Scatterplots of HWMs and peak hydrograph water levels (with locations shown in Fig. 2) compared with ADCIRC peak water levels; the subfigures show predictions with (a) HWind and (b) GAHM-BT (Note: Green points indicate a match within 0.5 m; orange, yellow, and light green circles indicate overprediction by the model; green, blue, dark blue, and purple circles indicate underpredictions); the zero-crossing slope of the best fit line and the R^2 value are indicated in each subfigure.

assimilated HWind product should be a better representation of the small-scale structures and asymmetric behavior of hurricanes. However, based on these results, the authors will use GAHM-BT as the best approximation of the true behavior of the winds and water levels as Isaac moved through the northern Gulf of Mexico.

Forecasts with GAHM Using NHC Guidance

To examine how the coupled SWAN + ADCIRC modeling system would perform as a forecast tool during the storm, the authors consider simulations that were initialized with the best available information at selected instances as the storm progressed through the Gulf of Mexico. Using GAHM forcing, the predictions are developed using parameters from 25 forecast advisories issued by the NHC. The forecasts start with Advisory 12, which was issued at 0300 UTC on August 24, 2012, and which has the storm approaching Mobile Bay (but not making landfall) within its 5-day forecast. The landfall location then shifted eastward into Florida for the next several advisories. The forecasts end with Advisory 36, which was issued at 0300 UTC on August 30, 2012, when the storm center had moved inland and halfway to Baton Rouge. By the end of this 5-day forecast, the storm had moved into Ohio. The storm tracks for these 25 forecasts are shown in Fig. 7. To highlight the changing storm surge impact in southeastern Louisiana, the authors show results from three forecasts: GAHM-21, initiated at 0900 UTC on August 26, 2012, about 63 h before initial landfall; GAHM-25, initiated at 0900 UTC on August 27, 2012, about 39 h before initial landfall; and GAHM-29, initiated at 0900 UTC on August 28, 2012, about 15 h before initial landfall.

The atmospheric conditions changed quickly as the storm moved toward Louisiana. In GAHM-21, the predicted storm track had shifted westward so its landfall location was near Mobile Bay in southern Alabama [Figs. 8(a and b)]. The strongest wind speeds of about 40 m s^{-1} were predicted to occur along the storm track, and the wind speeds were about 10–15 m s^{-1} over much of Louisiana to the west of the Mississippi River. Compared with the GAHM-BT simulation, these wind speeds were too small by about 15–20 m s, underestimating the impact in Louisiana. Twenty-four hours later in GAHM-25, the predicted storm track had moved into southeastern Louisiana, but its intensity was too strong [Figs. 8(c and d)]. The strongest wind speeds were still about 40 m s^{-1} along a band to the northwest of the storm track, stretching from the Gulf over the Mississippi River and New Orleans. The wind speeds were reduced by ADCIRC in overland regions to account for the surface roughness. Even so, the maximum wind speeds were too large by about 10 m s^{-1} over Lakes Borgne and Pontchartrain, compared with GAHM-BT. In the span of 24 h between GAHM-21 and GAHM-25, the predicted wind hazards had changed completely for southern Louisiana, with the track shifting from Alabama to Louisiana, with the marine wind speeds of 15–20 m s^{-1} increasing to 35–40 m s^{-1}.

In the later GAHM-29, the storm track shifted a bit farther to the west with a landfall location near Grand Isle, and its peak winds of about 35 m s^{-1} were smaller and contained to the west of the Mississippi River [Figs. 8(e and f)]. Although the peak winds were slightly overpredicted by about 5 m s^{-1} compared with GAHM-BT, the maximum wind speeds were underpredicted by about 5 m s^{-1} in regions away from the storm track, such as the continental shelf between Louisiana and Mississippi. This simulation, based on forecast guidance issued about 15 h before the storm's initial landfall, is the closest match to the true wind hazards during the storm.

It is important to note that these differences relative to GAHM-BT also show errors associated with the predicted forward speed of the storm, in addition to errors associated with its track and intensity. Isaac was a slow-moving storm, especially as it made landfall. This slow forward speed can allow winds to push surge for a longer time, allowing larger water levels along the coast. This behavior is evident in the maximum water levels for these three advisories. In GAHM-21, the northerly winds caused the water levels to be elevated by about 1 m along the levees of the Mississippi River Gulf Outlet and the Mississippi River, but the water levels were too low by more than 2 m throughout southern Louisiana [Figs. 9(a and b)]. By GAHM-25, the region was impacted by severe hazards of 3–4 m in the Caernarvon and Biloxi marshes to the east of the city of New Orleans, and more than 2 m in Lake Pontchartrain [Figs. 9(c and d)]. These predicted water levels were too high by about 0.5 m to the east-northeast of the city, due to the storm tracking too close to these regions. The predicted water levels were too low by 1–1.5 m in the Caernarvon Marsh, and especially in the marshes to the south of the city. These underpredictions were likely caused by a combination of errors in the storm track and forward speed, i.e., the storm was moving too closely to the city and not pushing enough surge into the marshes to the west of the river.

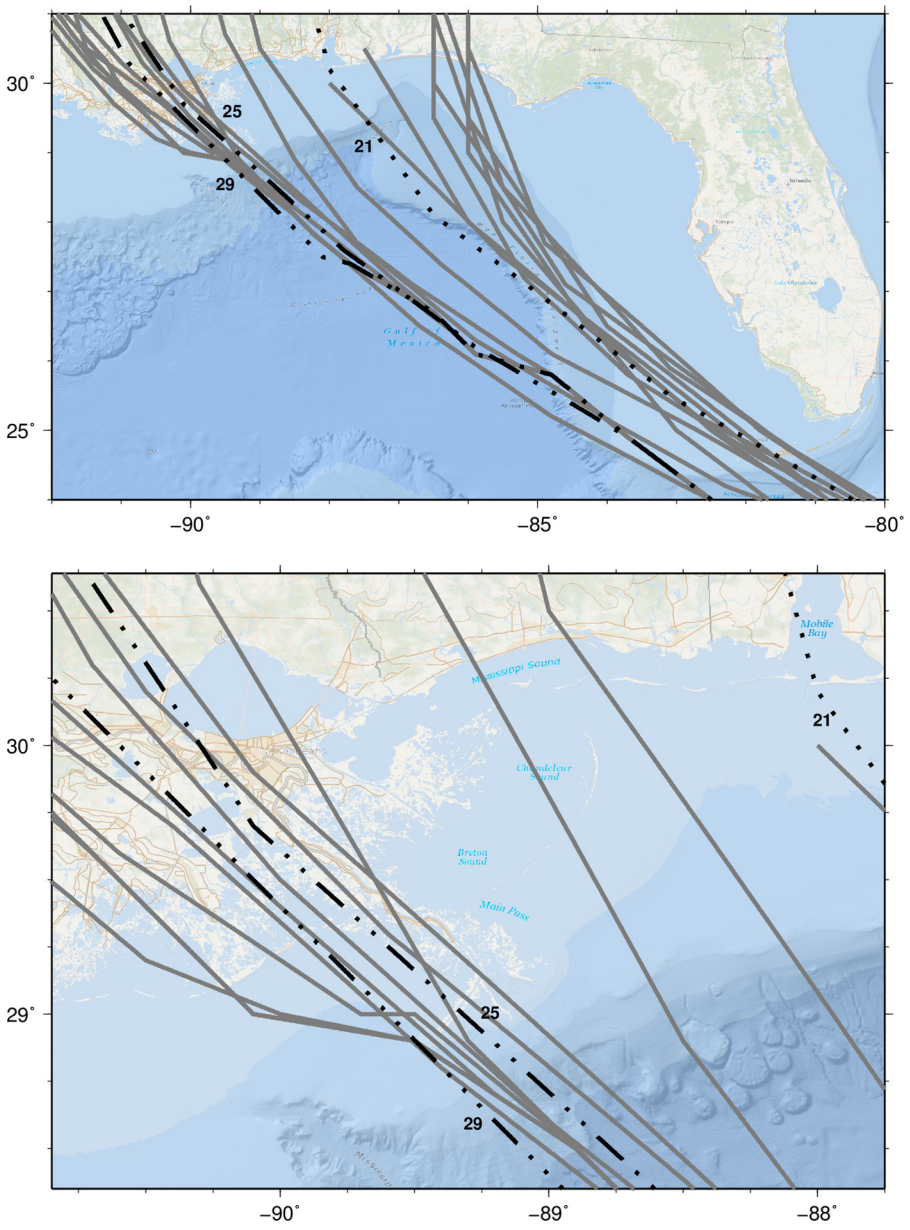

Fig. 7. (Color) NHC 120-h forecast tracks for Advisories 12–36 during Isaac [Note: Tracks for Advisories 21 (dotted), 25 (dot-dot-dashed), and 29 (dot-dot-dot-dashed) are identified and labeled in black; all other advisories are shown in solid gray]; tracks for earlier Advisories 12–20 had landfall locations in the Florida panhandle, whereas tracks after Advisory 25 had landfall locations in southeastern Louisiana

By GAHM-29, the maximum water levels had decreased somewhat, with peak values of about 3.5 m along the levees near New Orleans, but smaller water levels in the marshes and Lake Pontchartrain [Figs. 9(e and f)]. These water levels are too low by about 0.5 m, with a consistent underprediction throughout southern Louisiana, which was likely due to the faster forward speed in the forecast guidance. The storm track for this forecast [i.e., Fig. 9(e), dotted line] is a close match to the BT guidance (i.e., Fig. 2, solid line), but it does not include the slow meandering of the storm offshore of Grand Isle in the 8 h between its two landfalls. This slowdown allowed winds to push more surge into the marshes south and east of the city. Even in this late advisory, the flooding hazards on the south side of the city are not predicted fully.

The changing surge hazard in southern Louisiana can also be computed as the RMS error in maximum water level between each advisory and the BT, for model vertices with bathymetric depths less than 10 m (Fig. 10). For Hurricane Gustav (2008), which had a landfall location that varied within a spread of about 60 km, the RMS errors had a downward trend of –0.186 m day^{-1} during the last 3 days of the storm (Forbes et al. 2010). For Isaac, the RMS errors converge rapidly as the storm track shifted toward Louisiana. For Advisories 21–25, the errors decreased at a rate of –1.07 m/day, or more than five times faster than during Gustav, but before and after those advisories, the RMS differences are almost constant. The hazards changed quickly for southeastern Louisiana.

Analyses of Selected Forecasts with GAHM and UWIN-CM

The wind and surge hazards were different between forecasts issued about 2.5 and 1.5 days before initial landfall and depended on atmospheric forcing sources. These changes are evident in GAHM-

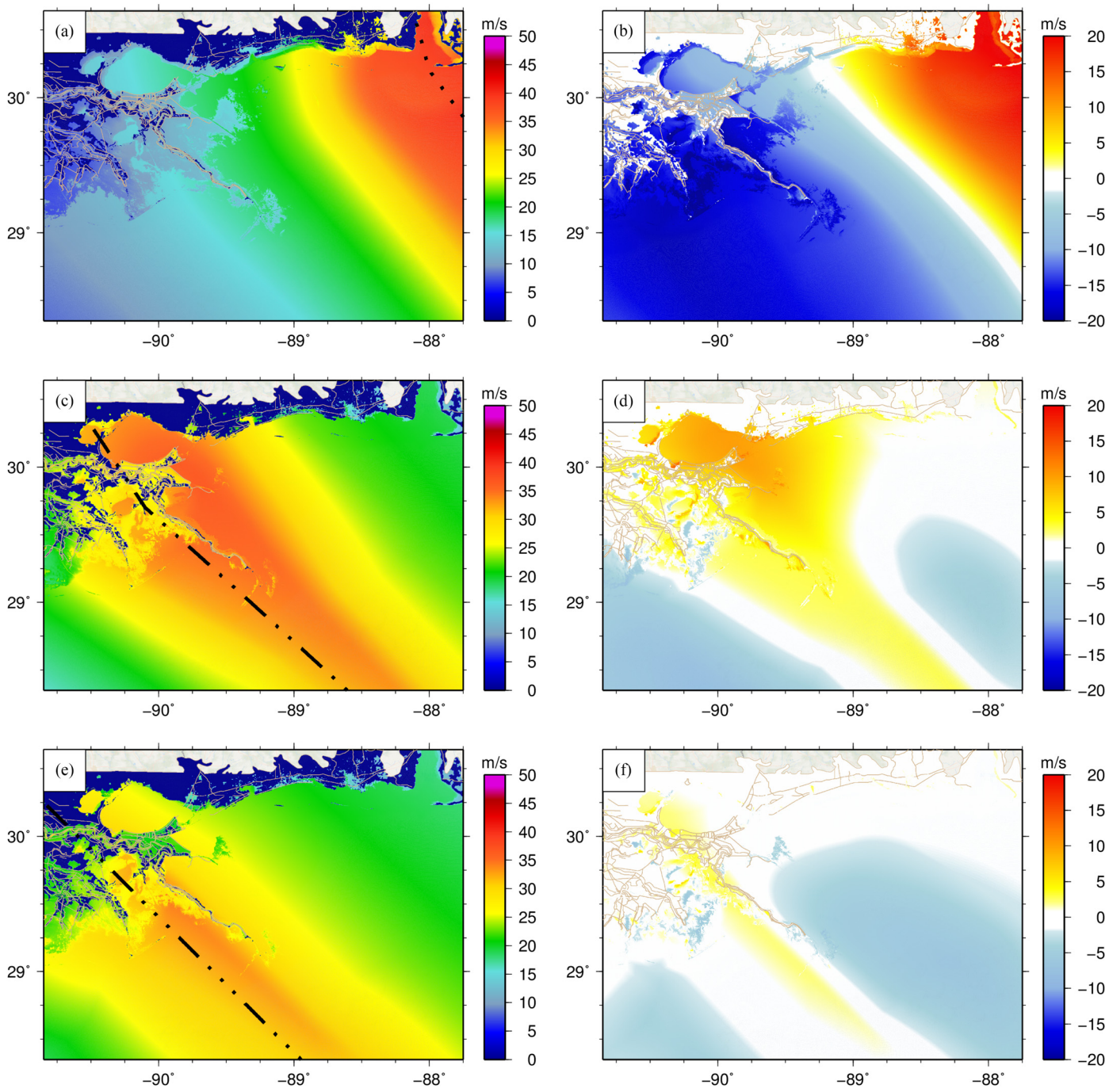

Fig. 8. (Color) Contours of (a, c, and e) maximum wind speeds (m s^{-1}) and (b, d, and f) differences in maximum wind speeds (m s^{-1}) during Isaac; differences are relative to the GAHM-BT simulation [Note: Results and storm tracks for (a and b) GAHM-21 (dotted), (c and d) GAHM-25 (dot-dot-dashed), and (e and f) GAHM-29 (dot-dot-dot-dashed) are shown]

21 and GAHM-25, which are based on a parametric wind model and the NHC advisories. The authors can compare these with simulations from the full-physics coupled model to examine the small-scale differences in the atmospheric forcing and ocean response as the storm approached and moved through southeastern Louisiana. These are compared with UWIN-CM simulations initialized at similar advisories: UWIN-CM-21a, issued at 1200 UTC on August 26, 2012, about 60 h before initial landfall, and UWIN-CM-25a, issued at 1200 UTC on August 27, 2012, about 36 h before initial landfall. These simulations are also compared with a slower version of this latter forecast, in which the storm is slowed by 6 h as it progresses through the system to better match the timing of the landfall in the NHC BT guidance. This simulation is denoted as UWIN-CM-25a + 6 h. Then, to illustrate the meteorological forcing and its effects on coastal flooding throughout the system, the authors examined two selected dates/times during the storm: 1600 UTC on August 28, 2012, or about 8 h before initial landfall, as the storm was located offshore of the Mississippi River Delta and transitioning into hurricane status, and 0800 UTC on August 29, 2012, as the storm was making its second landfall near Grand Isle, Louisiana.

As Isaac moved through the Gulf of Mexico, its central pressure was relatively low, but it lacked a well-defined eye, which delayed

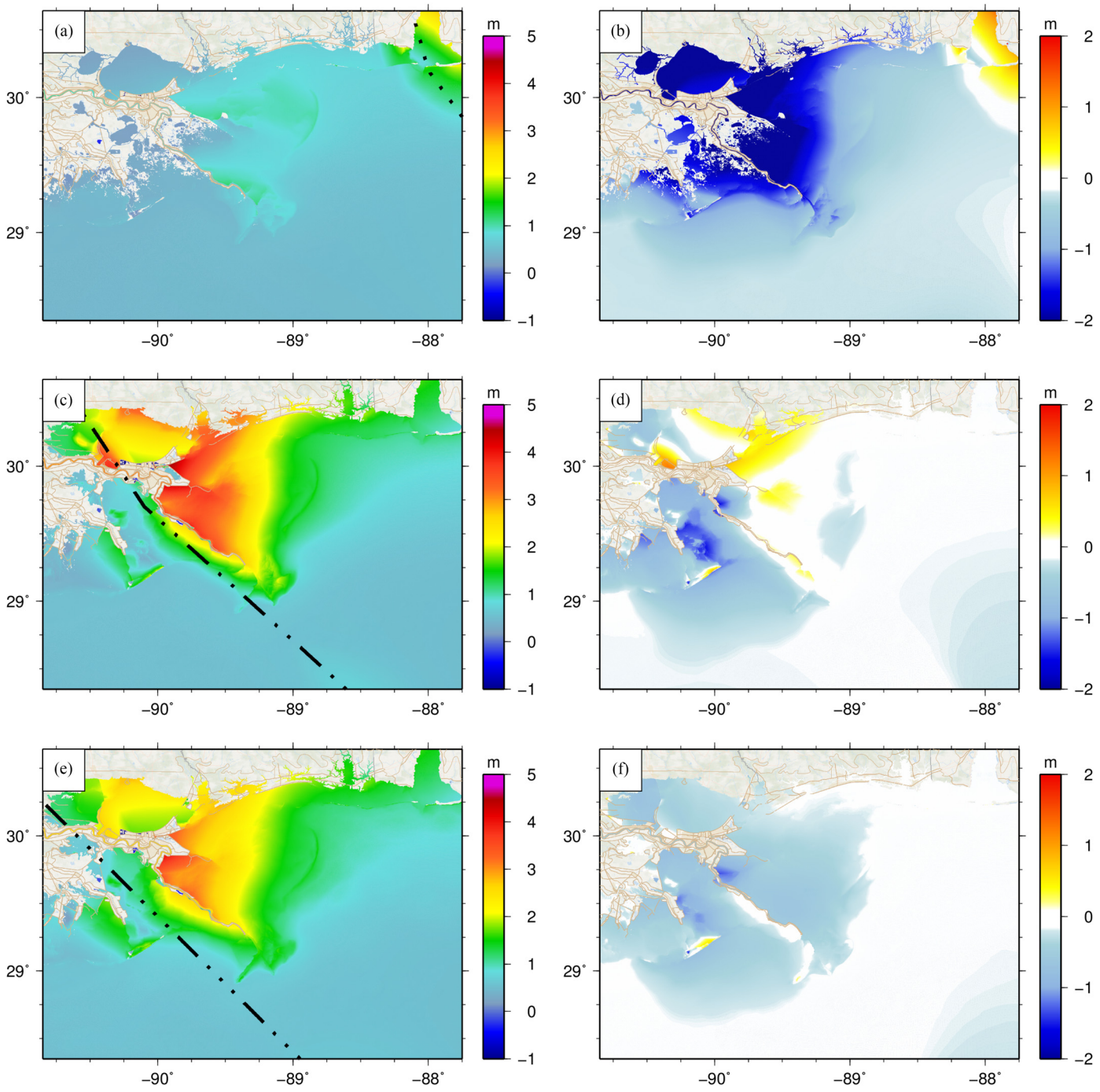

Fig. 9. (Color) (a, c, and e) Contours of maximum water levels (m relative to NAVD88) and (b, d, and f) differences in maximum water levels (m) during Isaac [Note: Differences are relative to the GAHM-BT simulation; results and storm tracks for (a and b) GAHM-21 (dotted), (c and d) GAHM-25 (dot-dot-dashed), and (e and f) GAHM-29 (dot-dot-dot-dashed) are shown]

its classification as a hurricane until only about 12 h before its initial landfall in Louisiana. It is a challenge to represent this disorganization with numerical models (Fig. 11). GAHM predicts smooth fields for barometric pressures and wind speeds at 1600 UTC on August 28, 2012, as the storm was transitioning into hurricane status. For UWIN-CM-21a, the landfall location was nearly correct, but the storm was projected to turn north-northeastward and move over the marshes east of New Orleans. The storm track projection were more accurate in UWIN-CM-25a, although the wind fields are broader in both predictions than the corresponding GAHM wind fields, with hurricane wind speeds extending to the river delta, and tropical storm-strength winds extending onto the Louisiana-Mississippi continental shelf. These wind fields are also broader than GAHM-BT, in which tropical storm-strength wind speeds greater than 25 m s^{-1} are located offshore. However, when the storm is slowed by 6 h in UWIN-CM-25a + 6 h, the wind field is a closer match to GAHM-BT, especially on the continental shelf and along the coasts of Louisiana and Mississippi, in which the wind speeds should be 20 m s^{-1} or less.

These differences in meteorological predictions lead to differences in the predicted water levels during Isaac (Fig. 12). For GAHM,

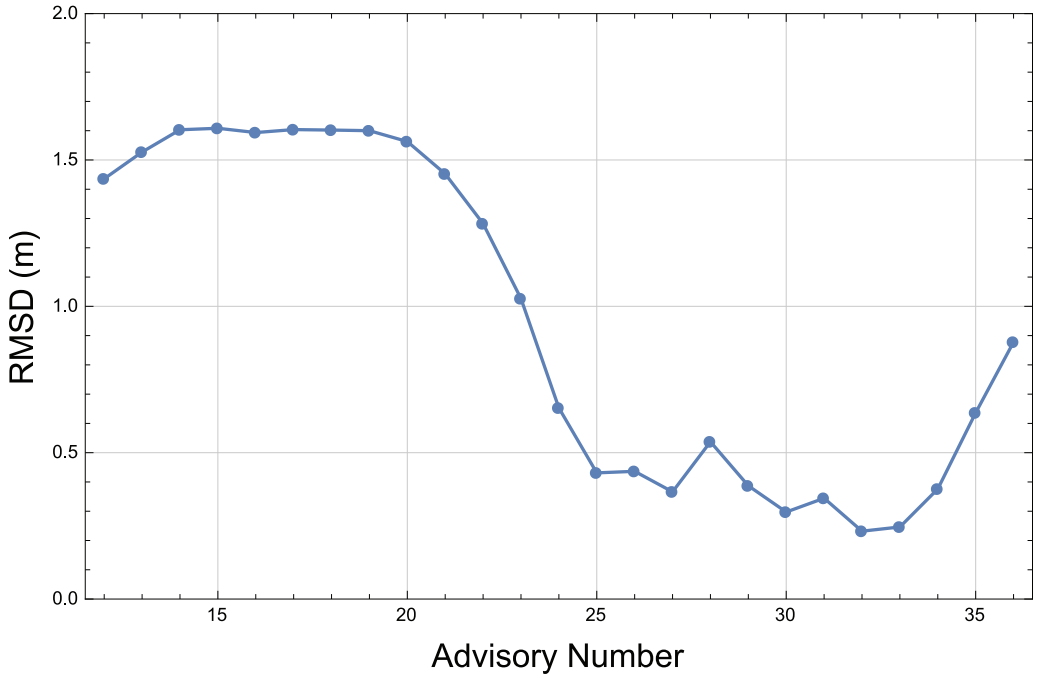

Fig. 10. (Color) RMS errors in maximum water elevation between each advisory and the BT at each model vertex for depths less than 10 m

its varying landfall locations caused the winds to be directed differently over southeastern Louisiana at 1600 UTC on August 28, 2012. The water levels throughout the region are well predicted during GAHM-25, compared with GAHM-BT. In the UWIN-CM-21a forecast, the storm tracked in a northward direction after landfall and passed east of New Orleans, impacting the water levels on the Louisiana-Mississippi shelf. Surge was pushed against the Mississippi River levees in which the water levels were about 2–2.5 m over much of the Caernarvon Marsh, and water levels were raised above 1 m throughout the Mississippi Sound and into Mobile Bay. In UWIN-CM-25a, the storm tracked to the west of New Orleans but was broader, increasing the surge on the shelf. The water levels were almost 3 m along the Mississippi River at 1600 UTC on August 28, 2012, and high water levels of 2–2.5 m pushed northward to the Mississippi coastline. This behavior is corrected in UWIN-CM-25a + 6 h, in which the predicted water levels are a closer match to GAHM-BT, with magnitudes of 1–2 m behind the barrier islands and northward.

Sixteen hours later at 0800 UTC on August 29, 2012, the storm was making its second landfall near Grand Isle, Louisiana (Fig. 13). For GAHM-21, the storm moved over Mobile Bay. At locations in Louisiana, the winds had speeds of 10 to 20 m s^{-1} and were directed offshore. For GAHM-25, the storm was moved too far inland with its eye located over New Orleans. The tropical storm-strength wind speeds greater than 25 m s^{-1} extended throughout Louisiana and onto the continental shelf. These predictions showed a storm that was too strong and moving too fast. For UWIN-CM-21a, the eye was larger and located farther to the southwest, closer to its true location. The largest wind speeds (greater than 25 m s^{-1}) were contained near the eye and did not extend beyond the Mississippi River. For UWIN-CM-25a, the storm had moved too far inland with its eye located southwest of New Orleans, but its wind field extended farther over the Louisiana-Mississippi continental shelf, with pockets of tropical storm-strength wind speeds greater than 25 m s^{-1} along the Mississippi coastline. To minimize the effect of this faster forward speed, this simulation was slowed down by 6 h as UWIN-CM-25a + 6 h [Fig. 13(f)]. For this slower forecast, the storm center location is a close match to GAHM-BT, but the winds are stronger by about 5 m s^{-1} near the storm center and to the south and west of the Mississippi River.

The easterly and southeasterly winds were sustained over the Louisiana-Mississippi continental shelf and pushed storm surge over the marshes and bayous to the east of metropolitan New Orleans (Fig. 14). This behavior was missed entirely by GAHM-21, but it was replicated for the later GAHM-25. At this time, the water levels were higher than 4 m over the Caernarvon and Biloxi marshes, and surge was threatening the levees along English Turn and the confluence of the Mississippi River Gulf Outlet and Gulf Intracoastal Waterway. To the west of the storm track, northwesterly winds were pushing water away from Terrebonne Bay, in which the water levels experienced a drawdown of more than 1 m. The more compact wind field and faster forward speed for the UWIN-CM forecasts resulted in lesser surge development throughout the region. The water levels in the Caernarvon Marsh had a maximum of about 3.5 m, whereas Biloxi Marsh and the levee system experienced water levels between 2–3 m. However, when the storm is delayed in UWIN-CM-25a + 6 h, the surge development is more accurate in the Biloxi marsh and in the confluence of the manufactured waterways to the east of New Orleans. The winds were also easterly and southeasterly over the Louisiana-Mississippi continental shelf, but their smaller magnitudes led to smaller surge. For all wind models, however, ADCIRC predicted similar surges of 1–2 m along the Mississippi and Alabama coasts.

During Isaac at the eight meteorological stations (Table 3), the GAHM forecasts showed a slight underprediction in the atmospheric pressures, whereas the UWIN-CM forecasts showed a slight overprediction. The RMS errors in the atmospheric pressures are smaller for the UWIN-CM (about 3 hPa) than for the GAHM (about 14 hPa), and the errors in the wind speeds were also smaller (by as much as 2.5 m s^{-1}). These error statistics are increased slightly when all 40 stations are considered; the errors in atmospheric pressures are about 11–14 hPa for the GAHM and about 3–4 hPa for the UWIN-CM, and the errors in the wind speeds are about 4–6 m s^{-1}. These errors are significant when compared with the maximum

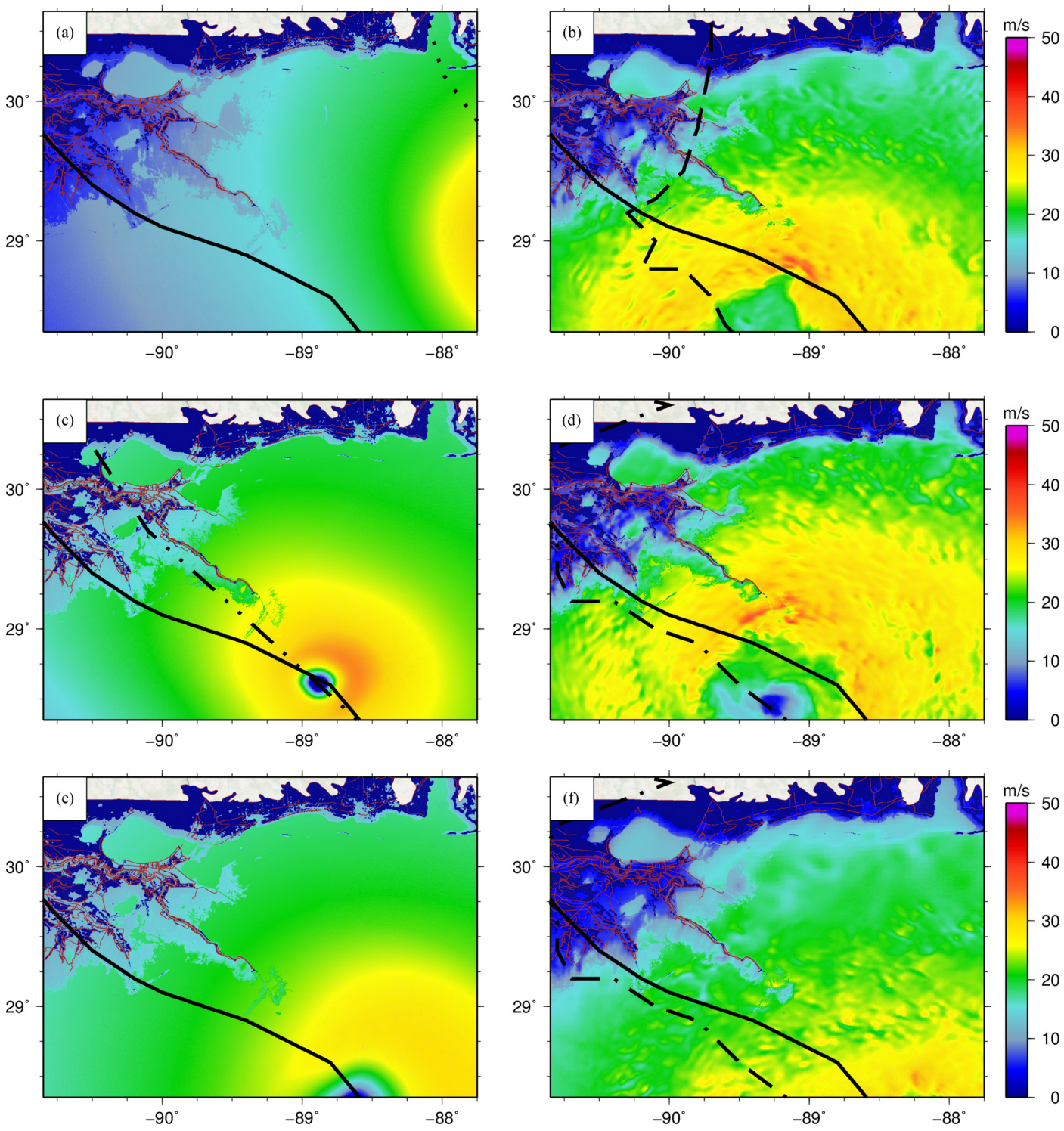

Fig. 11. (Color) Wind speeds (m s^{-1}) corresponding to 1600 UTC on August 28, 2012, as Isaac transitioned into hurricane status [Note: Subfigures show predictions and storm tracks for (a) GAHM-21 (dotted), (b) UWIN-CM-21a (dashed), (c) GAHM-25 (dot-dot-dashed), (d) UWIN-CM-25a (dot-dash-dashed), (e) GAHM-BT (solid), and (f) UWIN-CM-25a + 6h (dot-dash-dashed)]

pressure deficit (about 50 hPa) and maximum wind speed (about 33 m s^{-1}). It is noted that the UWIN-CM-25a model predictions compare favorably with GAHM-BT, with smaller errors in atmospheric pressures (2.35 hPa compared with 3.70 hPa) and smaller errors in wind speeds (by about 0.5 m s^{-1}). The errors are slightly worse for UWIN-CM-25a + 6 h, but are still better than for GAHM-BT.

At the 12 hydrograph locations (Table 4), the errors improve during the later advisory for the water levels predicted with forcing from the GAHM; the RMS error improves from 0.94 to 0.42 m. For the water levels predicted with forcing from the UWIN-CM, the errors are consistent between the two initializations, with RMS errors of about 0.46 m, similar to the GAHM-25 simulation. These errors are consistent when considering all 112 stations and

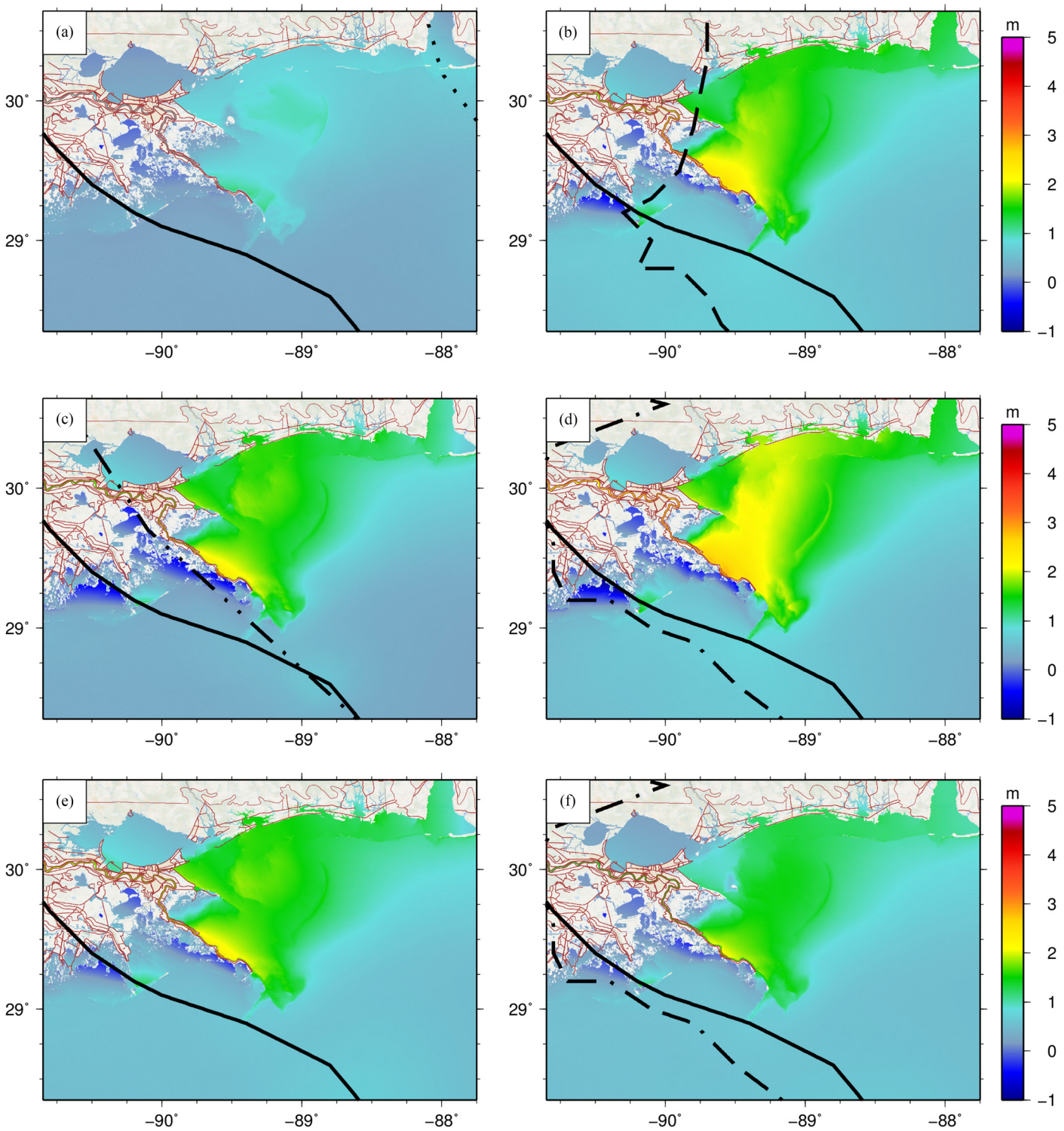

Fig. 12. (Color) Water levels (meters relative to NAVD88) predicted by ADCIRC corresponding to 1600 UTC on August 28, 2012, as Isaac transitioned into hurricane status [Note: Subfigures show predictions and storm tracks for (a) GAHM-21 (dotted), (b) UWIN-CM-21a (dashed), (c) GAHM-25 (dot-dot-dashed), (d) UWIN-CM-25a (dot-dash-dashed), (e) GAHM-BT (solid), and (f) UWIN-CM-25a + 6h (dot-dash-dashed)]

gauges. There is a noticeable improvement in the error statistics for GAHM-BT; the RMS error is reduced to about 0.27– 0.35 m. The best performance is from the full-physics, slowed down UWIN-CM-25a + 6 h simulation, which has RMS errors of 0.20–0.26 m, indicating its skill in forcing storm surge through this region.

These peak water levels can be compared with observations of HWMs and peak hydrograph water levels during the storm. In addition to the 112 time series observations described previously, the USGS collected 103 HWMs in Alabama, Mississippi, and Louisiana (McCallum et al. 2012). Three of these HWMs were discarded as outliers. The remaining 212 observed peak values (with

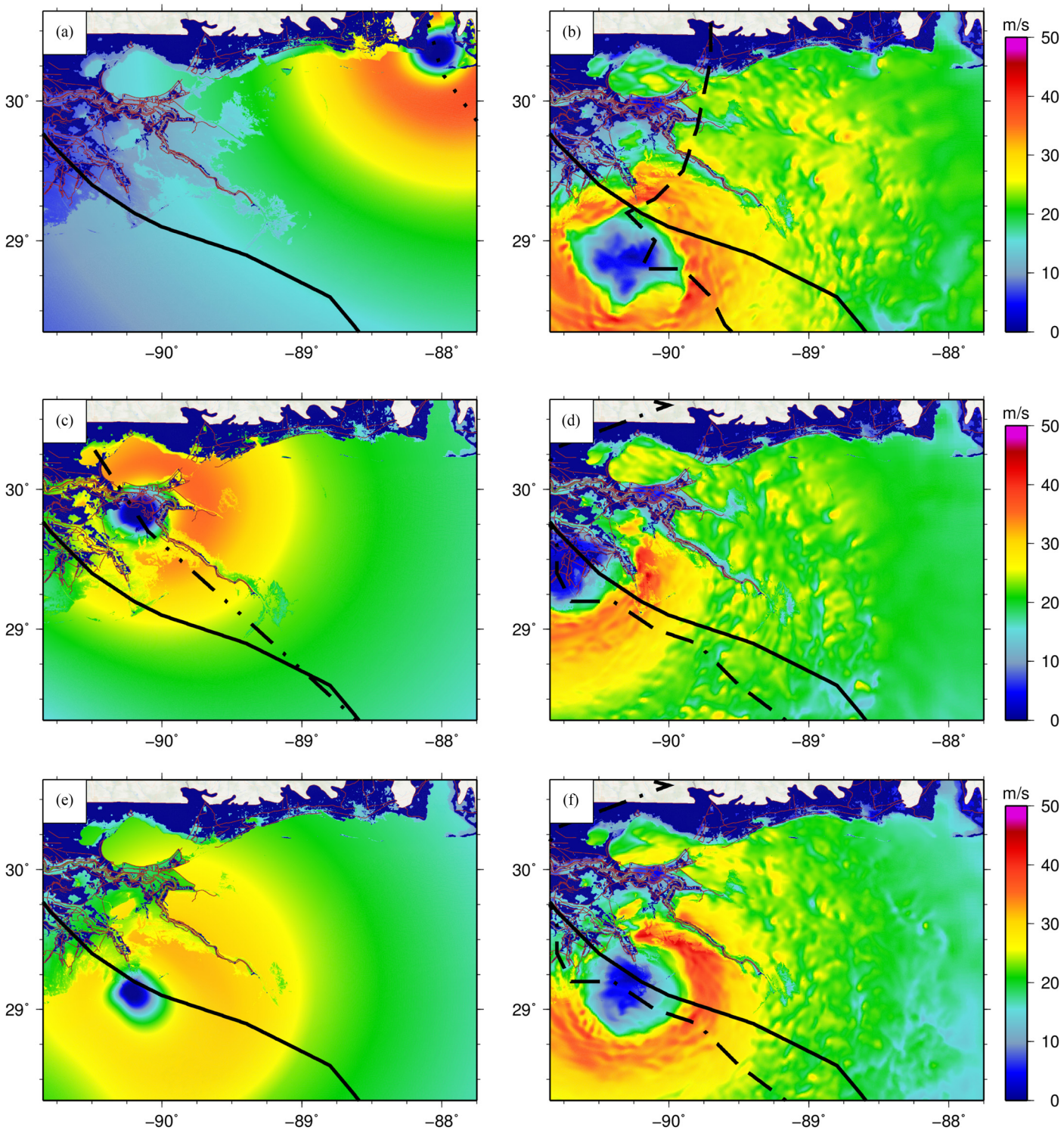

Fig. 13. (Color) Wind speeds (m s^{-1}) corresponding to 0800 UTC on August 29, 2012, as Isaac was making its second landfall near Grand Isle, Louisiana [Note: Subfigures show predictions and storm tracks for (a) GAHM-21 (dotted), (b) UWIN-CM-21a (dashed), (c) GAHM-25 (dot-dot-dashed), (d) UWIN-CM-25a (dot-dash-dashed), (e) GAHM-BT (solid), and (f) UWIN-CM-25a + 6h (dot-dash-dashed)]

locations shown in Fig. 2) were compared with ADCIRC model predictions (in scatterplots shown in Fig. 15). With forcing from GAHM-25, the peak water levels from ADCIRC were a good match to the observations, with a zero-crossing best fit slope of $m = 0.99$ and $R^2 = 0.49$, and the modeled peak water levels were within 0.5 m at 68% of the HWMs and peak hydrograph values. With forcing from the UWIN-CM-25a, the peak water levels were biased to underprediction but showed a better overall match to the observations, with a zero-crossing best fit slope of $m = 0.92$ and $R^2 = 0.59$, and the modeled peak water levels were within 0.5 m at 79% of the HWMs and peak hydrograph values. These values are slightly better than the ADCIRC model performance when using GAHM-BT, suggesting that the additional complexity of the UWIN-CM can offset some of the uncertainties in its storm size and track.

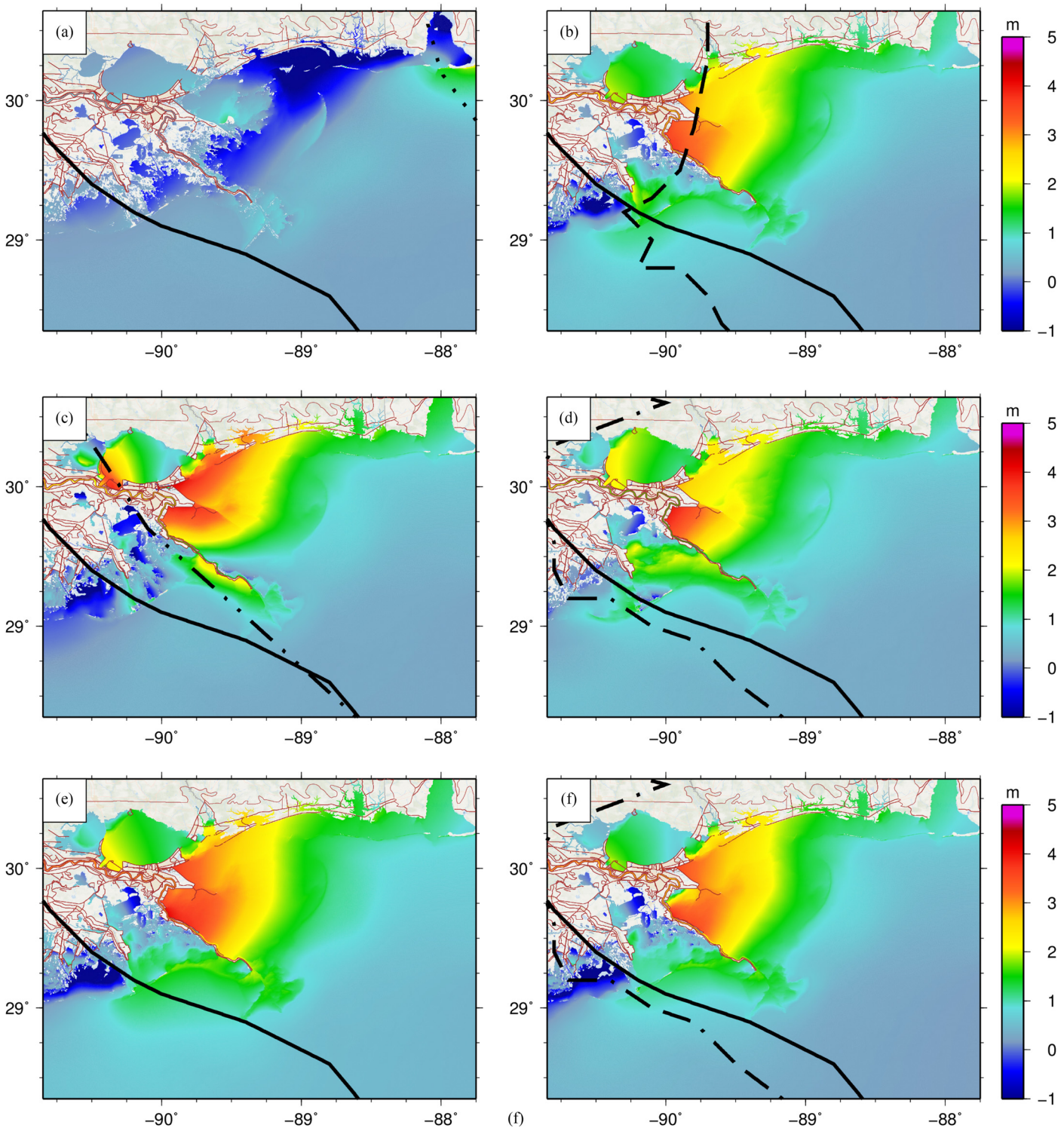

Fig. 14. (Color) Water levels (meters relative to NAVD88) predicted by ADCIRC corresponding to 0800 UTC on August 29, 2012, as Isaac was making its second landfall near Grand Isle, Louisiana [Note: Subfigures show predictions and storm tracks for (a) GAHM-21 (dotted), (b) UWIN-CM-21a (dashed), (c) GAHM-25 (dot-dot-dashed), (d) UWIN-CM-25a (dot-dash-dashed), (e) GAHM-BT (solid), and (f) UWIN-CM-25a + 6h (dot-dash-dashed)]

Conclusions

The SWAN + ADCIRC modeling system was applied to high-resolution simulations of storm surge and flooding during Hurricane Isaac (2012). The surge model was forced with forecasts of surface pressure and wind fields from an analysis product, HWind, and two atmospheric models, GAHM and UWIN-CM. The effects of the atmospheric forcing were evaluated for hindcasts using the best available information after the storm, and then for forecasts as the storm moved through the Gulf and approached southeastern Louisiana. Predictions of surface pressures and wind speeds were compared with observations at 40 stations, whereas predictions of water levels were

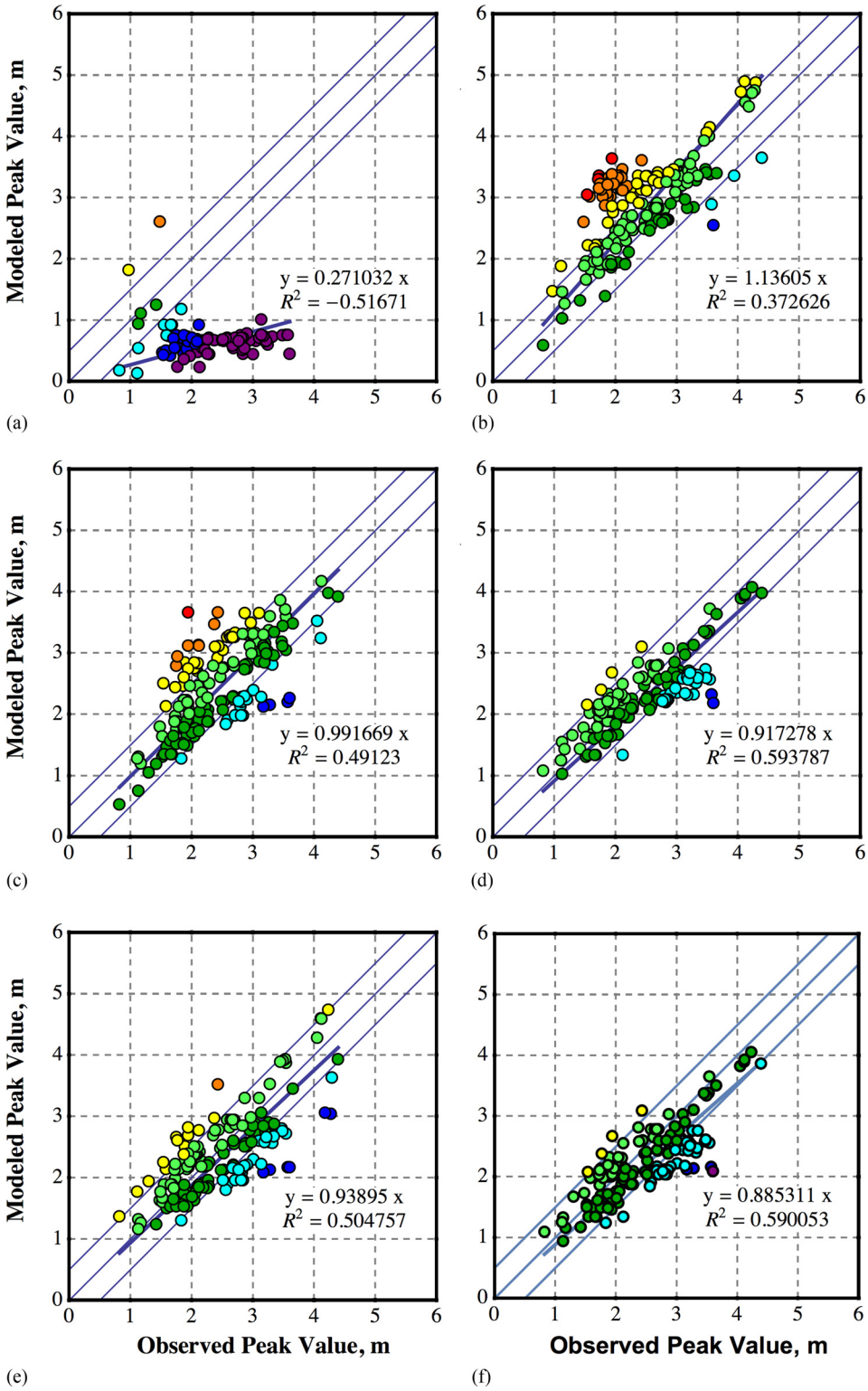

Fig. 15. (Color) Scatterplots of HWMs and peak hydrograph water levels (with locations shown in Fig. 2) compared with ADCIRC peak water levels; subfigures show predictions with (a) GAHM-21, (b) UWIN-CM-21a, (c) GAHM-25, (d) UWIN-CM-25a, (e) GAHM-BT, and (f) UWIN-CM-25a + 6h (Note: Green points indicate a match within 0.5 m; red, orange, yellow, and light green circles indicate overprediction by the model; green, blue, dark blue, and purple circles indicate underpredictions); the zero-crossing slope of the best fit line and the R^2 value are indicated in each subfigure

compared with observations at 112 stations in the region. The findings can be summarized as follows:

1. The GAHM-BT hindcast was a better representation than HWind of Isaac's wind hazards and associated ocean response. The parametric vortex model used information from the BT advisory to generate spatially and temporally varying fields for surface pressures and wind velocities, and these fields were a better match to observations and led to a more accurate storm

surge. The GAHM-BT hindcast was used as a baseline for comparisons with the surge forecasts.

2. Given realistic forecast advisories, the GAHM parametric vortex model gave realistic forecasts of storm surge for Isaac, suggesting its value for real-time forecast applications. For the earlier GAHM forecasts in which the storm was projected to make landfall along the Florida panhandle, the ADCIRC water levels were too small throughout southeastern Louisiana, Mississippi, and Alabama. The surge predictions improved considerably for the later forecasts in which the storm track was projected more accurately through Louisiana, with errors caused primarily by the storm moving too fast and not pushing enough surge over the marshes to the southeast of New Orleans. These analyses demonstrate the considerable sensitivity of the surge model predictions to the hurricane forecast. When GAHM receives storm parameters that are realistic, then its relative efficiency allows for faster predictions with accuracy comparable to data-assimilated products and full-physics atmospheric models.
3. UWIN-CM provided an improved forecast skill at least 24 h earlier than the forecast advisories, which translated to improved skill in forecasting storm surge. Although common wisdom is that forecast advisories consistently outperform individual models, this is a contrary example. UWIN-CM predicted the storm to move through southern Louisiana, even in its earlier forecasts, so the early surge predictions with long lead times were improved when forced with its results compared with those using the NHC advisory forecast track. Even with timing errors due to the storm forward speed, the surge model predictions were generally good when forced with results from UWIN-CM, with RMS errors comparable to the BT simulation. When the timing errors were minimized by slowing down the storm by 6 h, the water-level predictions improved significantly to be lower than the BT simulation. These findings are encouraging in terms of demonstrating the forecast skill (in terms of both wind and storm surge) of a full-physics atmospheric model coupled with a high-resolution storm surge model.

Although this study is specific to Isaac, it demonstrates its potential for more accurate forecasts, especially in long lead times. The authors are encouraged to continue to develop a fully coupled, dynamic model for tropical cyclones, waves, and storm surge for future coastal hazard forecast applications. Future work will include a tighter coupling between the UWIN-CM atmospheric forcing and the SWAN + ADCIRC modeling system, with the goal of providing forecast guidance about storm surge and flooding in the coastal environment.

Acknowledgments

This research was made possible by a grant from the Gulf of Mexico Research Initiative. Data are publicly available through the Gulf of Mexico Research Initiative Information & Data Cooperative (GRIIDC) at https://data.gulfresearchinitiative.org and with the following Digital Object Identifiers (DOIs): 10.7266/N7QR4V62, (Dietrich et al. 2017a), 10.7266/N7GB2251 (Dietrich et al. 2017b), and 10.7266/N7BK19F9 (Dietrich et al. 2017c).

References

Battjes, J. A., and Janssen, J. P. F. M. (1978). "Energy loss and set-up due to breaking of random waves." *Proc., 16th Int. Conf. on Coastal Engineering*, ASCE, Reston, VA, 569–587.

Berg, R. (2013). "Tropical cyclone rep., Hurricane Isaac, 21 August–1 September 2012." National Hurricane Center, Miami.

Beven, J. L., and Kimberlain, T. B. (2009). "Tropical cyclone report, Hurricane Gustav, 25 August–4 September 2008." National Hurricane Center, Miami.

Black, P. G., et al. (2007). "Air–sea exchange in hurricanes: Synthesis of observations from the coupled boundary layer air-sea transfer experiment." *Bull. Am. Meteorol. Soc.*, 88(3), 357–374.

Blanton, B. O., et al. (2012). "Urgent computing of storm surge for North Carolina's coast." *Procedia Computer Sci.*, Vol. 9, 1677–1686.

Booij, N., Ris, R. C, and Holthuijsen, L. H. (1999). "A third-generation wave model for coastal regions: 1. Model description and validation." *J. Geophys. Res.*, 104(C4), 7649–7666.

Bretschneider, C. L., Krock, H. J., Nakazaki, E., and Casciano, F. M. (1986). "Roughness of typical Hawaiian terrain for tsunami runup calculations: A user's manual." *J.K.K. Look Laboratory Rep.*, Univ. of Hawaii, Honolulu.

Bunya, S., et al. (2010). "A high-resolution coupled riverine flow, tide, wind, wind wave, and storm surge model for southern Louisiana and Mississippi: Part I: Model development and validation." *Mon. Weather Rev.*, 138(2), 345–377.

Cavaleri, L., and Malanotte-Rizzoli, P. (1981). "Wind wave prediction in shallow water: Theory and applications." *J. Geophys. Res.*, 86(C11), 10961–10973.

Chen, S. S., and Curcic, M. (2016). "Ocean surface waves in Hurricane Ike (2008) and Superstorm Sandy (2012): Coupled model predictions and observations." *Ocean Modell.*, 103(Jul), 161–176.

Chen, S. S., Price, J. F., Zhao, W., Donelan, M. A., and Walsh, E. J. (2007). "The CBLAST-Hurricane program and the next-generation fully coupled atmosphere-wave-ocean models for hurricane research and prediction." *Bull. Am. Meteorol. Soc.*, 88, 311–317.

Chen, S. S., Zhao, W., Donelan, M. A., and Tolman, H. L. (2013). "Directional wind-wave coupling in fully coupled atmosphere-wave-ocean models: Results from CBLAST-hurricane." *J. Atmos. Sci.*, 70, 3198–3215.

Cheung, K. F., et al. (2003). "Modeling of storm-induced coastal flooding for emergency management." *Ocean Eng.*, 30(11), 1353–1386.

Cyriac, R., Dietrich, J. C., Fleming, J. G., Blanton, B. O., Kaiser, C., Dawson, C. N., and Luettich, R. A. (2017). "Variability in coastal flooding predictions due to forecast errors during Hurricane Arthur (2014)." *Coastal Eng.*, in press.

Dawson, C. N., Westerink, J. J., Feyen, J. C., and Pothina, D. (2006). "Continuous, discontinuous and coupled discontinuous-continuous Galerkin finite element methods for the shallow water equations." *Int. J. Numer. Methods Fluids*, 52(1), 63–88.

Dietrich, J. C., et al. (2010). "A high-resolution coupled riverine flow, tide, wind, wind wave, and storm surge model for southern Louisiana and Mississippi. Part II: Synoptic description and analysis of Hurricanes Katrina and Rita." *Mon. Weather Rev.*, 138(2), 378–404.

Dietrich, J. C., et al. (2017a). "CARTHE-II: SWAN+ADCIRC forecast and hindcast simulations of Hurricane Isaac (2012) using GAHM." Gulf of Mexico Research Initiative Information and Data Cooperative (GRIIDC), Harte Research Institute, Texas A&M Univ., College Station, TX.

Dietrich, J. C., et al. (2017b). "CARTHE-II: SWAN+ADCIRC forecast simulations of Hurricane Isaac (2012) using UWIN-CM." Gulf of Mexico Research Initiative Information and Data Cooperative (GRIIDC), Harte Research Institute, Texas A&M Univ., College Station, TX.

Dietrich, J. C., et al. (2017c). "CARTHE-II: SWAN+ADCIRC hindcast simulation of Hurricane Isaac (2012) using HWind." Gulf of Mexico Research Initiative Information and Data Cooperative (GRIIDC), Harte Research Institute, Texas A&M Univ., College Station, TX.

Dietrich, J. C., et al. (2012a). "Performance of the unstructured-mesh, SWAN+ADCIRC model in computing hurricane waves and surge." *J. Sci. Comput.*, 52, 468–497.

Dietrich, J. C., et al. (2012b). "Surface trajectories of oil transport along the northern coastline of the Gulf of Mexico." *Cont. Shelf Res.*, 41, 17–47.

Dietrich, J. C., et al. (2011a). "Hurricane Gustav (2008) waves and storm surge: Hindcast, validation and synoptic analysis in southern Louisiana." *Mon. Weather Rev.*, 139(8), 2488–2522.

Dietrich, J. C., et al. (2011b). "Modeling hurricane waves and storm surge using integrally-coupled, scalable computations." *Coastal Eng.*, 58, 45–65.
Dietrich, J. C., et al. (2013). "Limiters for spectral propagation velocities in SWAN." *Ocean Modell.*, 70(Oct), 85–102.
DiNapoli, S. M., Bourassa, M. A., and Powell, M. D. (2012). "Uncertainty and intercalibration analysis of H*Wind." *J. Oceanic Atmos. Technol.*, 29(6), 822–833.
Donelan, M. A., Curcic, M., Chen, S. S., and Magnusson, A. K. (2012). "Modeling waves and wind stress." *J. Geophys. Res.*, 117(C11), C00J23.
Dresback, K. M., et al. (2013). "Skill assessment of a real-time forecast system utilizing a coupled hydrologic and coastal hydrodynamic model during Hurricane Irene (2011)." *Cont. Shelf Res.*, 71(Dec), 78–94.
Ebersole, B. A., Westerink, J. J., Resio, D. T., and Dean, R. G. (2007). "Performance evaluation of the New Orleans and Southeast Louisiana hurricane protection system, Vol. IV–The storm." *Final Rep. of the Interagency Performance Evaluation Task Force*, U.S. Army Corps of Engineers, Washington, DC.
Fleming, J., Fulcher, C., Luettich, R., Estrade, B., Allen, G., and Winer, H. (2008). "A real time storm surge forecasting system using ADCIRC." *Estuarine and Coastal Model.*, 893–912.
Forbes, C., Luettich, R. A., Mattocks, C. A., and Westerink, J. J. (2010). "A retrospective evaluation of the storm surge produced by Hurricane Gustav (2008): Forecast and hindcast results." *Weather Forecasting*, 25(6), 1577–1602.
Forbes, C., and Rhome, J. (2012). "Initial tests of an automated operational storm surge prediction system for the National Hurricane Center." *Proc., 30th Conf. on Hurricanes and Tropical Meteorology*, American Meteorological Society, Boston.
Gao, J., Luettich, R. A., and Fleming, J. G. (2017). "Development and evaluation of a generalized asymmetric tropical cyclone vortex model in ADCIRC." *ADCIRC Users Group Meeting*, U.S. States Army Corps of Engineers, Vicksburg, MS.
Garratt, J. R. (1977). "Review of drag coefficients over oceans and continents." *Mon. Weather Rev.*, 105, 915–929.
Glahn, B., Taylor, A., Kurkowski, N., and Shaffer, W. A. (2009). "The role of the SLOSH model in National Weather Service storm surge forecasting." *National Weather Digest*, 33, 3–14.
Hasselmann, S., Hasselmann, K., Allender, J. H., and Barnett, T. P. (1985). "Computations and parameterizations of the nonlinear energy transfer in a gravity wave spectrum, part II: Parameterizations of the nonlinear transfer for application in wave models." *J. Phys. Oceanogr.*, 15, 1378–1391.
Holland, R. W. (1980). "An analytic model of the wind and pressure profiles in hurricanes." *Mon. Weather Rev.*, 108, 1212–1218.
Hope, M. E., et al. (2013). "Hindcast and validation of Hurricane Ike (2008) waves, forerunner, and storm surge." *J. Geophys. Res. C: Oceans*, 118(9), 4424–4460.
Hu, K., Chen, Q., and Kimball, K. S. (2012). "Consistency in hurricane surface wind forecasting: An improved parametric model." *Nat. Hazards*, 61(3), 1029–1050.
Hu, K., Chen, Q., and Wang, H. (2015). "A numerical study of vegetation impact on reducing storm surge by wetlands in a semi-enclosed estuary." *Coastal Eng.*, 95, 66–76.
Irish, J. L., Resio, D. T., and Cialone, M. A. (2009). "A surge response function approach to coastal hazard assessment, part 2: Quantification of spatial attributes of response functions." *Nat. Hazards*, 51(1), 183–205.
Judt, F., Chen, S. S., and Berner, J. (2016). "Predictability of tropical cyclone intensity: Scale-dependent forecast error growth in high-resolution stochastic kinetic-energy backscatter ensembles." *Q. J. Roy. Meteorol. Soc.*, 142(694), 43–57.
Kennedy, A. B., et al. (2012). "Tropical cyclone inundation potential on the Hawaiian islands of Oahu and Kauai." *Ocean Model.*, 52–53, 54–68.
Kerr, P., et al. (2013). "Surge generation mechanisms in the lower Mississippi River and discharge dependency." *J. Waterway, Port, Coastal, Ocean Eng.*, 10.1061/(ASCE)WW.1943-5460.0000185, 326–335.
Kerr, P. C., et al. (2015). "US IOOS coastal and ocean modeling testbed: Evaluation of tide, wave, and hurricane surge response sensitivities to mesh resolution and friction in the Gulf of Mexico." *J. Geophys. Res. C: Oceans*, 118, 4633–4661.
Kinnmark, I. (1986). *The shallow water wave equations: Formulation, analysis and application*, Springer-Verlag, Berlin.
Knabb, R. D., Rhome, J. R., and Brown, D. P. (2005). "Tropical cyclone report., Hurricane Katrina, 23-30 August 2005." National Hurricane Center, Miami.
Kolar, R. L., Westerink, J. J., Cantekin, M. E., and Blain, C. A. (1994). "Aspects of nonlinear simulations using shallow-water models based on the wave continuity equation." *Comput. Fluids*, 23(3), 1–24.
Komen, G. J., Hasselmann, S., and Hasselmann, K. (1984). "On the existence of a fully developed wind-sea spectrum." *J. Phys. Oceanogr*, 14(8), 1271–1285.
Luettich, R. A., and Westerink, J. J. (2004). "Formulation and numerical implementation of the 2D/3D ADCIRC finite element model version 44. XX." ⟨http://adcirc.org/adcirc_theory_2004_12_08.pdf⟩ (Sep. 18, 2017).
Madsen, O. S., Poon, Y. K., and Graber, H. C. (1988). "Spectral wave attenuation by bottom friction: Theory." *Proc., 21st Int. Conf. on Coastal Engineering*, ASCE, Reston, VA, 492–504.
Martyr, R., et al. (2013). "Simulating hurricane storm surge in the lower Mississippi River under varying flow conditions." *J. Hydraul. Eng.*, 10.1061/(ASCE)HY.1943-7900.0000699, 492–501.
Mattocks, C., and Forbes, C. (2008). "A real-time, event-triggered storm surge forecasting system for the state of North Carolina." *Ocean Model.*, 25(3–4), 95–119.
McCallum, B. E., et al. (2012). "Monitoring storm tide and flooding from Hurricane Isaac along the Gulf Coast of the United States, August 2012." *Rep. No. 20121263*, USGS, Reston, VA.
Powell, M. D. (2006). "National Oceanic and Atmospheric Administration (NOAA) Joint Hurricane Testbed (JHT) program." *Final Rep.*, National Oceanic and Atmospheric Administration, Silver Spring, MD.
Powell, M. D., and Houston, S. H. (1996). "Hurricane Andrew's Landfall in South Florida. Part II: Surface wind fields and potential real-time applications." *Weather Forecasting*, 11, 329–349.
Powell, M. D., Houston, S. H., Amat, L. R., and Morisseau-Leroy, N. (1998). "The HRD real-time hurricane wind analysis system." *J. Wind Eng. Ind. Aerodyn.*, 77–78, 53–64.
Resio, D. T., and Westerink, J. J. (2008). "Modeling of the physics of storm surges." *Phys. Today*, 61(9), 33–38.
Ris, R. C., Booij, N., and Holthuijsen, L. H. (1999). "A third-generation wave model for coastal regions: 2. Verification." *J. Geophys. Res.*, 104(C4), 7667–7681.
Rogers, W. E., Hwang, P. A., and Wang, D. W. (2003). "Investigation of wave growth and decay in the SWAN model: Three regional-scale applications." *J. Phys. Oceanogr.*, 33, 366–389.
Schloemer, R. W. (1954). "Analysis and synthesis of hurricane wind patterns over Lake Okeechobee, FL." *Rep. No. 31*, Government Printing Office, Washington, DC.
Skamarock, W. C., et al. (2008). "A description of the Advanced Research WRF Version 3." *NCAR Technical Notes, NCAR/TN-4751STR*, National Center for Atmospheric Research, Boulder, CO.
Snyder, R. L., Dobson, F. W., Elliott, J. A., and Long, R. B. (1981). "Array measurements of atmospheric pressure fluctuations above surface gravity waves." *J. Fluid Mech.*, 102, 1–59.
Taflanidis, A., et al. (2013a). "Rapid assessment of wave and surge risk during landfalling hurricanes; probabilistic approach." *J. Waterway Port Coastal, Ocean Eng.*, 10.1061/(ASCE)WW.1943-5460.0000178, 171–182.
Taflanidis, A. A., Jia, G., Kennedy, A. B., and Smith, J. M. (2013b). "Implementation/optimization of moving least squares response surfaces for approximation of hurricane/storm surge and wave responses." *Nat. Hazards*, 66(2), 955–983.
Tanaka, S., Bunya, S., Westerink, J. J., Dawson, C., and Luettich, R. A. (2011). "Scalability of an unstructured grid continuous Galerkin based hurricane storm surge model." *J. Sci. Comput.*, 46(3), 329–358.
USACE (U.S. Army Corps of Engineers). (2015). "North Atlantic coast comprehensive study: Resilient adaption to increasing risk, main report." ⟨http://www.nad.usace.army.mil/Portals/40/docs/NACCS/NACCS_main_report.pdf⟩ (Sep. 18, 2017).
Wallcraft, A. J., Metzger, E. J., and Carroll, S. N. (2009). "Software design description for the HYbrid Coordinate Ocean Model (HYCOM) version 2.2." *Rep. No. NRL/MR/732009-9166*, Naval Research Laboratory, Washington, DC.

Wamsley, T. V., Cialone, M. A., Smith, J. M., Atkinson, J. H., and Rosati, J. D. (2010). "The potential of wetlands in reducing storm surge." *Ocean Eng.*, 37(1), 59–68.

Westerink, J. J. (2008). "Flood insurance study: Southeastern parishes, Louisiana, intermediate submission 2: Offshore water levels and waves." FEMA, U.S. Army Corps of Engineers, Washington, DC.

Westerink, J. J., et al. (2008). "A basin to channel scale unstructured grid hurricane storm surge model applied to Southern Louisiana." *Mon. Weather Rev.*, 136, 833–864.

Xie, L., Bao, S., Pietrafesa, L. J., Foley, K., and Fuentes, M. (2006). "A real-time hurricane surface wind forecasting model: Formulation and verification." *Mon. Weather Rev.*, 134, 1355–1370.

Zachry, B. C., Booth, W. J., Rhome, J. R., and Sharon, T. M. (2015). "A national view of storm surge risk and inundation." *Weather Clim. Soc.*, 7, 109–117.

Zijlema, M. (2010). "Computation of wind-wave spectra in coastal waters with SWAN on unstructured grids." *Coastal Eng.*, 57(3), 267–277.